Ore Geology Reviews 131 (2021) 104042

Contents lists available at ScienceDirect

Ore Geology Reviews

journal homepage: www.elsevier.com/locate/oregeorev

Petrogenesis of Zr–Nb (REE) carbonatites from the Arbarastakh complex (Aldan Shield, Russia): Mineralogy and inclusion data

I.R. Prokopyev [a,b,*], A.G. Doroshkevich [a,c], D.V. Zhumadilova [a], A.E. Starikova [a,b], Ya. N. Nugumanova [a,b], N.V. Vladykin [d]

[a] Sobolev Institute of Geology and Mineralogy Siberian Branch Russian Academy of Sciences, Russia
[b] Department of Geology and Geophysics, Novosibirsk State University, Russia
[c] Geological Institute Siberian Branch Russian Academy of Sciences, Russia
[d] A.P. Vinogradov Institute of Geochemistry Siberian Branch Russian Academy of Sciences, Russia

ARTICLE INFO

Keywords:
Carbonatites
Phoscorites
Aldan shield
Siberian craton

ABSTRACT

The Arbarastakh Neoproterozoic ultramafic carbonatite complex is located in the southwestern part of the Siberian Craton (Aldan Shield) and contains ore-bearing Zr–Nb (REE) carbonatites and phoscorites. Carbonatites are mainly represented by calcite and silicocarbonatite varieties. The primary minerals composing the carbonatites are calcite and dolomite, as well as phlogopite, clinopyroxene, fluorapatite, amphibole, fluorite, K-feldspar and feldspathoids. Olivine (forsterite), Ti-magnetite, apatite, phlogopite, calcite, dolomite and the minor spinel group minerals form the primary phoscorites. The ore-bearing Zr–Nb mineral assemblages of the phoscorites and carbonatites include accessory zircon, zirconolite, perovskite, pyrochlore and baddeleyite. The Ba–Sr–REE hydrothermal mineralisation consists of ancylite-(Ce), bastnaesite-(Ce) and burbankite, as well as barite-celestite, strontianite, barytocalcite, and rare Cu–Fe sulphides. The silicocarbonatites and carbonatites formed in multiple stages from a single alkaline Ca–Na–K–silicocarbonatite melt, while the phoscorites are products of differentiation of the carbonatitic melt and were crystallised from an Fe-rich phosphate–carbonate melt at temperatures of more than 720 °C. The silicate–phosphate–carbonate melts were responsible for the Zr–Nb mineralisation of the carbonatites at temperatures of more than 540–575 °C; the hydrothermal REE-bearing mineral assemblages crystallised from saline (60–70 wt%) carbonatitic fluids of Na–Ca–Mg–F–carbonate composition at a minimum temperature range of 350–300 °C. The Ca–Sr-carbonate as well as the Na–hydro–carbonate fluids were responsible for the Ba–Sr–REE mineralisation of the phoscorites at ~500–480 and 450–430 °C.

1. Introduction

Ultramafic carbonatite complexes are a unique group of igneous rocks carrying information about the deep magma processes which generate specific compositions of alkaline silicate and carbonate melts, as well as about carbon cycle processes and metasomatism in the mantle. Carbonatite melts are formed by differentiation of carbonated alkaline nephelinite (or syenite) magmas, as a result of silicate–carbonate immiscibility processes, and by the direct mantle melting of magnesiocarbonatites (Rock, 1986; Le Bas, 1987; Woolley and Kempe, 1989; Dalton and Wood, 1993; Hamilton and Kjarsgaard, 1993; Kogarko et al., 1995; Mitchell, 1995, 2006; Tappe et al., 2005, 2006; Guzmics and Zajacz, 2013).

A wide range of ore deposits of various types, which are strategically important for high-tech modern industry, are associated with the alkaline carbonatite complexes: rare metals (Nb, Zr, Ta, etc.), rare earth elements (REE: La, Ce, Nd, etc.), radioactive metals (Th and U) and noble metals (Au, Ag, Pt), as well as iron, apatite, fluorite and other useful materials (e.g. Wall and Zaitsev, 2004; Chakhmouradian, 2006; Chakhmouradian and Wall, 2012; Wall, 2013; Smith et al., 2014; Chakhmouradian et al., 2015; Weng et al., 2015). Today, carbonatites are the primary global source of REEs and Nb, but the scale of the accumulation of rare metals differs significantly between different alkaline complexes, and there is currently no satisfactory explanation for these differences. A statistical summary of 527 known carbonatites (Woolley and Kjarsgaard, 2008) shows that only 45 show potential for

* Corresponding author at: Sobolev Institute of Geology and Mineralogy Siberian Branch Russian Academy of Sciences, Russia.
E-mail address: prokop@igm.nsc.ru (I.R. Prokopyev).

https://doi.org/10.1016/j.oregeorev.2021.104042
Received 24 September 2020; Received in revised form 21 January 2021; Accepted 26 January 2021
Available online 2 February 2021

mining. The processes of rare metal accumulation in carbonatites are still not fully explained.

According to the International Union of Geological Sciences (IUGS) classification of igneous rocks, phoscorite is "a magnetite, olivine, apatite rock usually associated with carbonatites" (Le Maitre, 2002). About twenty-one well-known ultramafic carbonatite complexes in the world (e.g. Palabora in South Africa and Kovdor in Russia) are spatially and temporally associated with and genetically related to phoscorites, which are potential sources for complex Fe–P, Nb–Ta–Zr, REE and Cu ores (Bulakh et al., 2004; Krasnova et al., 2004a, 2004b; Wall and Zaitsev, 2004). The majority of ore-bearing phoscorites are associated with occurrences of calcite and dolomite carbonatites (Krasnova et al., 2004b), and many of these complexes have not been fully described at present. The genetic relationship between carbonatites and phoscorites is the subject of debate, and currently three main mechanisms for the genesis of phoscorites have been proposed: (1) crystallisation from their own melt, (2) fractional crystallisation from a carbonatitic melt, and (3) separation from an immiscible carbonatitic melt (Krasnova et al., 2004b).

Carbonate–silicate immiscibility processes are involved in the formation of ore-bearing carbonatite complexes with Nb, Zr, and REE mineralisation (e.g. Bell et al., 1998; Belov et al., 2008). However, recent experimental data show that the distribution coefficients of Nb, Ta, Hf and Zr between carbonate and silicate melts are less than 1, and therefore these elements cannot be concentrated in the carbonate melt compared to the silicate melt (Veksler et al., 2012).

Experimental, melt and fluid inclusion studies in carbonatite systems demonstrate that REE minerals generally nucleate as a product of fluid-induced REE redistribution within magmatic minerals such as apatite (Harlov et al., 2002; Harlov and Förster, 2004; Shironosova and Prokopyev, 2018, 2019). Fluids involved in the transportation and deposition of REEs have high activities of ligands (F, Cl, CO_2(L), SO_4) and brines (e.g. NaCl) (e.g. Williams-Jones et al., 2012; Tropper et al., 2011, 2013). The orthomagmatic fluids have the carbonate–fluoride–-chloride–sulphate composition with salt contents of more than 85 wt%, and are responsible for the REE ore-bearing mineralisation of the carbonatite complexes (e.g. Rankin, 2005; Xie et al., 2009; Doroshkevich et al., 2010; Cooper et al., 2015; Broom-Fendley et al., 2016, 2017; Prokopyev et al., 2016, 2017; Nikolenko et al., 2018; Zheng and Liu, 2019; Shu and Liu, 2019; Redina et al., 2020). Data about Th and U solubility are limited, but experiments show that the ore-forming fluids are commonly rich in acid anions (Cl^-, F^-, SO_4^{2+}) (e.g. Altmaier et al., 2004; Hetherington and Harlov, 2008).

The Arbarastakh ultramafic carbonatite complex is a potential candidate for mining ore-bearing materials from the complex U–Ta–Zr–Nb, Fe–P and REE mineralisation. The ores are confined to the carbonatite and phoscorite bodies within metasomatic zones of fenitisation and albitisation, and contain 0.2–1.2 wt% Nb_2O_5, 0.002–0.1% Ta_2O, 0.003–0.3% UO_2, and 0.005–0.03% ThO_2 (Goroshko and Guryanov, 2004). The associated ore components are barium, strontium, phosphorus, copper and REEs. Therefore, the study of the genesis, mineral composition and geochemical characteristics of alkaline rocks of the Arbarastakh complex is important both for scientific and applied technological applications.

Modern information on the Arbarastakh complex is limited due to its inaccessibility. Existing data on the geological structure and age of the alkaline rocks show the crystallisation ages to be 690 ± 28 Ma for ultramafic rocks and carbonatites, and 720 ± 28 Ma for phoscorites (K–Ar, phlogopite; Glagolev et al., 1974). The temporal characteristics of the rocks are consistent with Neoproterozoic epoch (725–630 Ma) manifestations of intraplate magmatism within the marginal regions of the Siberian Craton associated with superplume activity and the formation of ore-bearing alkaline ultramafic carbonatite complexes, such as Belaya Zima, Tagna, Zhidoy, Ingili and others (Yarmolyuk et al., 2005, Fig. 1). With these age estimates for the Arbarastakh ultramafic carbonatite complex (720-690 Ma) it likely belongs to the 720 Ma Irkutsk Large Igneous Province (LIP) that is reconstructed with the coeval Franklin LIP of northern Laurentia (Ernst et al., 2016). And this is consistent with a more general observation of a strong association between carbonatites and LIPs (Ernst and Bell, 2010).

In this paper, we present new data about petrography, mineralogy and origin of the ore-bearing carbonatites and phoscorites from the Arbarastakh complex using mineralogical data and investigations of melt, mineral and fluid inclusions to show specific features of the

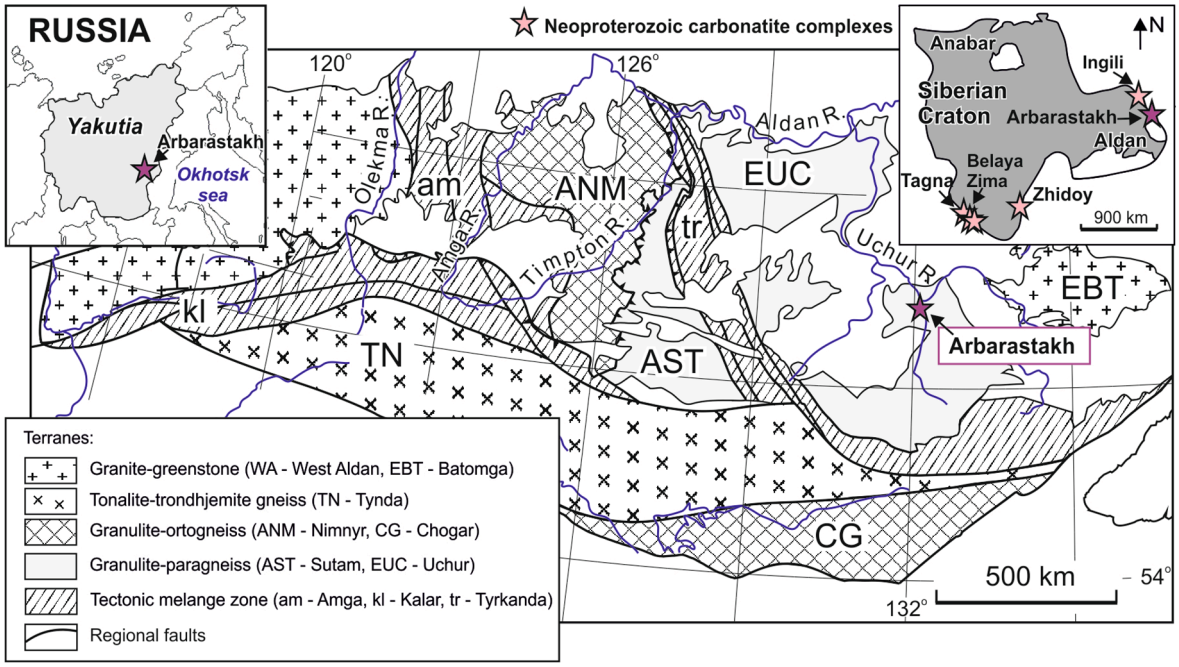

Fig. 1. Location of the Arbarastakh ultramafic carbonatite complex in the territory of Yakutia (Sakha Republic), south-eastern Russia (top left inset picture), and position of the Neoproterozoic carbonatite complexes within the marginal parts of the Siberian Craton (top right inset picture, after Ashchepkov et al., 2020). Terrane map of the Aldan Shield was modified after Parfenov and Kuzmin (2001).

petrogenesis of ore-bearing carbonatite complexes in the Siberian Craton at ca. 700–650 Ma.

2. Geological setting

2.1. Regional geology of the Aldan Shield

The Arbarastakh ultramafic carbonatite complex is located in the Sakha Republic (Yakutia) in south-eastern Russia, in the basin of the Arbarastakh River, a left tributary of the Idyum River (Lena River basin) (Fig. 1). Tectonically, the complex is situated in the eastern part of the Aldan Shield within the marginal region of the Siberian Craton, on the Uchur granulite-paragneiss terrane of the Siberian Craton (Fig. 1). The Arbarastakh alkaline complex covers an area of about 38 km^2 and was first investigated in the 1940s during a geological survey at a scale of 1:100 000 (Goroshko and Guryanov, 2004). A large number of local aerial uranium and thorium–uranium anomalies were revealed within the Arbarastakh complex in 1988. Later detailed geological investigations have provided revised estimates of the Nb-ore content of the Arbarastakh complex and made it possible to distinguish it as among the most promising structures in the southeast part of the Siberian platform (Goroshko and Guryanov, 2004).

The Siberian Craton consists of a series of accreted microcontinents such as Tungus, Anabar, Olenek, Aldan and Stanovoy, bounded by early Proterozoic orogenic fold belts (Rosen et al., 2002). The major crust-forming events within the Siberian Craton occurred at 3.5, 3.3, 3.0-2.5, 2.6-2.5, 2.15-1.95 and 1.9-1.85 Ga (Frost et al., 1998; Rosen et al., 2002; Priyatkina et al., 2020). The territory of the Aldan Shield is in the southern part of the Siberian Craton and is characterised by a complex structure (Fig. 1). The Aldan Shield is divided into the Aldan geoblock, as well as the Chara-Olekma and Batomgsky geoblocks to the west and east of the Aldan geoblock, respectively (Kotov et al., 2005, 2006, 2017). The Aldan geoblock is subdivided into the Western and Eastern Aldan megablocks and is composed almost entirely of metamorphosed rocks of the granulite facies.

The present data show that the Aldan Shield comprises five terranes, which are separated by tectonic mélange zones (Fig. 1; Parfenov and Kuzmin, 2001): West Aldan (WA), Nimnyr (ANM), Sutam (AST), Batomga (EBT) and Uchur (EUC). The central part of the Aldan Shield includes very widely spread Archean and Early Proterozoic granitoids, which are predominantly granite-gneisses. Five episodes of Early Precambrian intraplate magmatism, including A-type granitoids, are distinctly distinguished within the Aldan Shield and its folded frame and are dated to 2.62, 2.40–2.52, 2.07, 1.87–1.88 and 1.74–1.70 Ga (Velikoslavinskii, et al., 2011; Larin et al., 2012). These granitoids formed under intraplate conditions, but in different geodynamic settings: post-collisional lithosphere extension at 2.64 and 1.87–1.88 Ga, and anorogenic conditions (due to the activity of mantle plumes) at 2.40–2.52, 2.07 and 1.74–1.70 Ga (Larin et al., 2012).

2.2. Geology of the Arbarastakh complex

Previous petrological studies of the alkaline rocks of the Arbarastakh complex showed that the main phases are represented by pyroxenites, which are today classified as jacupirangites, cross-cutting bodies of carbonatites, phoscorites and ijolites, as well as outcrops of individual bodies of later alkaline syenites located along the periphery of the Arbarastakh complex (Glagolev et al., 1974) (Fig. 2). In previous works, outcrops of kimberlite-like bodies on the surface within the Arbarastakh complex were also noted (e.g. Goroshko and Guryanov, 2004); the present geological and petrographic studies have shown that these rocks can be attributed to ultramafic lamprophyre dikes according to the classification of Tappe et al. (2005) (Figs. 2 and 3).

The Archean bedrocks consist of biotite, diopside, hypersthene and hornblende crystalline schists, gneisses, amphibolites, garnet and graphite gneisses, marbles, and calc-silicate rocks (Parfenov and Kuzmin, 2001) (Fig. 2). The complex of sedimentary rocks is represented by Proterozoic arkoses, as well as dolomite and quartz sandstones with rare horizons of conglomerates and dolomites, which are located a few kilometres south and east from the contact of the Arbarastakh complex with the surrounding rocks (Glagolev et al., 1974).

Archean biotite–amphibole gneiss–granites (isolated complexes) and alaskite granites (migmatites and interstratal bodies) with a common north-eastern strike are widespread within the metamorphic sequence of bedrocks (Glagolev et al., 1974). The rocks form a series of narrow isoclinal folds falling in a northeast direction at a steep angle. This

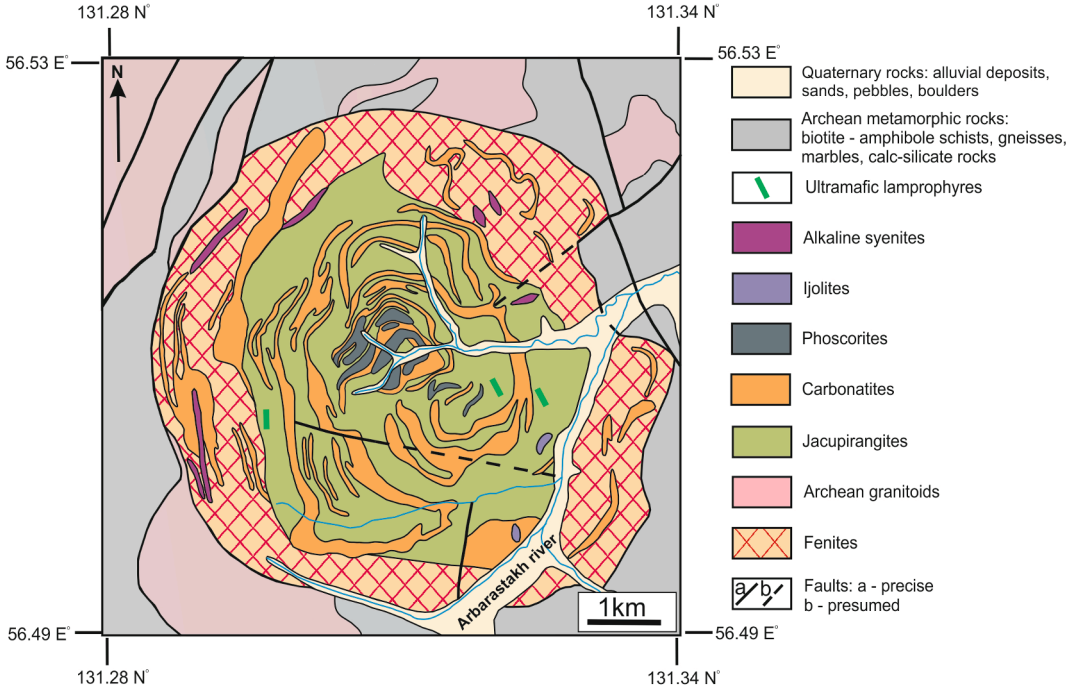

Fig. 2. Scheme of the geological structure of the Arbarastakh ultramafic carbonatite complex (modified after Glagolev et al. (1974)).

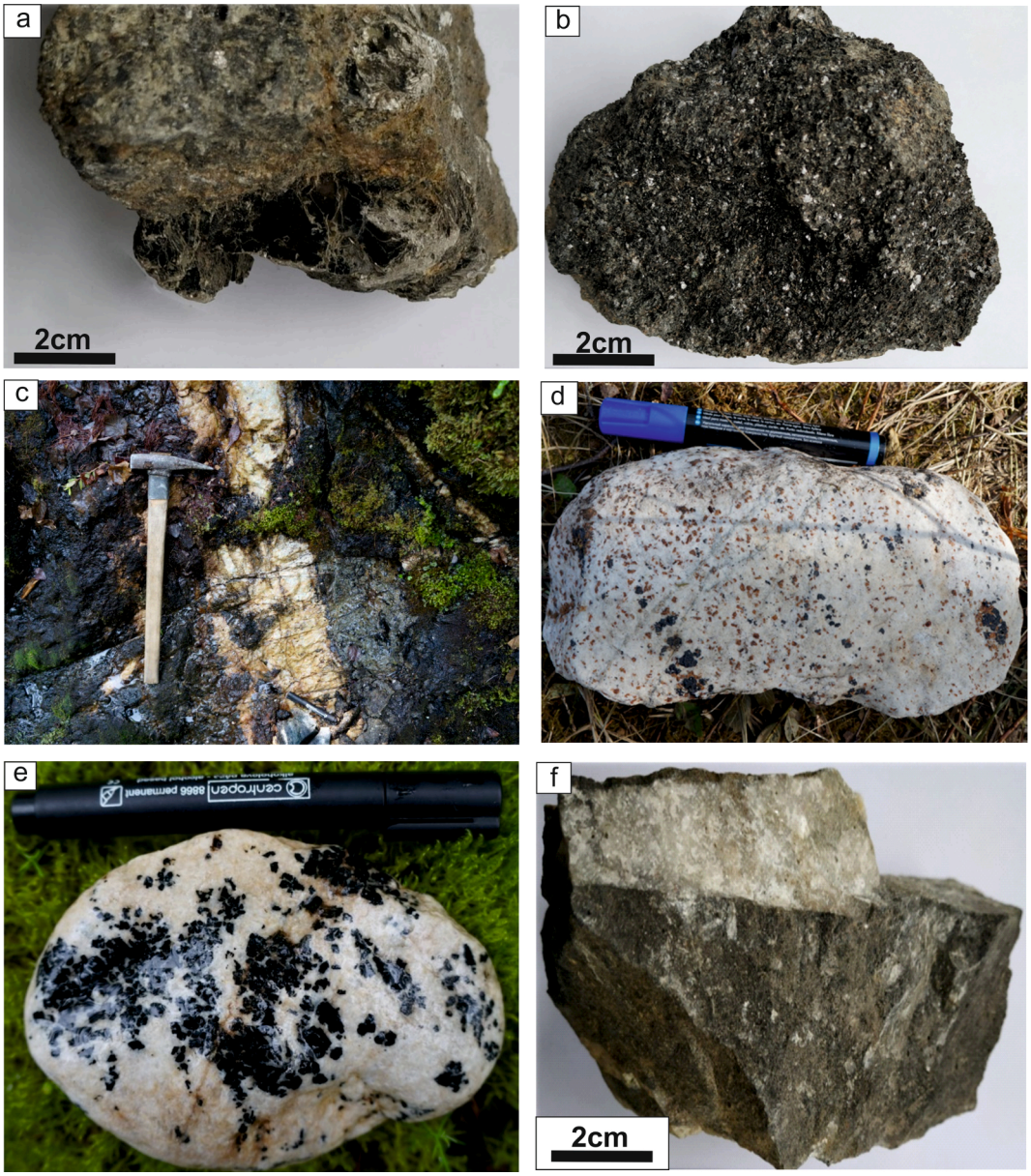

Fig. 3. Photographs of alkaline rocks from the Arbarastakh complex. Phlogopite-containing jacupirangite (a) and fenite from the contact zone containing nearly-monomineral aggregates of mica (b); carbonatite dike cross-cutting jacupirangites in an outcrop on the Arbarastakh River bank (c); pyrochlore- (d) and phlogopite-containing (e) carbonatites; sample from the contact of a carbonatite (white) with an ultramafic lamprophyre (grey) dike (f).

structure was formed in Archean time and most likely predetermined the appearance of the Arbarastakh complex in this place.

The main structural feature of the Arbarastakh complex is its concentric-zoned structure, expressed in the regular alternation of rocks with different compositions and different bedding conditions (Glagolev et al., 1974). The main phase of the complex is composed of a stock-shaped body of jacupirangites, which has a rounded ellipsoidal outline in plan and is elongated in the northwest direction (Fig. 2). The axes of the ellipse in the plan are about 6.7 and 6 km long. The body of jacupirangites has a roughly concentric structure and is composed of pyroxene, pyroxene–micaceous and pyroxene–hornblende rocks, sometimes containing albite, nepheline, cancrinite and other minerals. Between the body of jacupirangites and surrounding rocks there is a continuous zone of contact-metasomatic rocks—fenites (Figs. 2 and 3 a, b). The fenite zone is up to 1 km thick; the rocks are represented by altered phlogopite–pyroxene rocks in endocontact, and altered gneisses and carbonate rocks in exocontact.

The carbonatites of the Arbarastakh alkaline complex are concentrated inside the jacupirangite core and occur in the form of a series of incomplete conic dike-like bodies on the map (Fig. 2). Individual carbonatite bodies have thicknesses varying from 10 to 20 cm to 400 m, and secant contacts with jacupirangites (Fig. 3 c). Angles of incidence, regardless of proximity to the centre of the complex, are 60–80° to the centre of the complex (Glagolev et al., 1974). The most common calcite varieties of carbonatite contain pyrochlore, which is the main mineral phase of Nb, as well as silicate minerals (e.g. phlogopite and clinopyroxene) (Fig. 3 d, e). Veins (up to 1 m) of the later dolomite and ankerite carbonatites are also found in the jacupirangites.

In the central part of the Arbarastakh complex, the conical bodies of magnetite–apatite–forsterite rocks making contacts with the previously described phases are localised (Glagolev et al., 1974). These bodies are between 30 and 200 m in size (Fig. 2). According to modern classifications, the rocks were assigned to phoscorites (Wall and Zaitsev, 2004).

During field geological studies, we recorded three dikes of ultramafic

alkaline rocks in the central part of the complex, with a thickness of 1 m (Figs. 2 and 3 f). Dike bodies have contacts with carbonatites, and according to the classification of Tappe et al. (2005) can be attributed to ultramafic alkaline lamprophyres (damtjernites).

Dikes of alkaline syenites, as well as ijolite–urtites and melteigites, with thicknesses varying from a few cm to 50 m and lengths of up to 1 km, were intruded within the Arbarastakh complex (Glagolev et al., 1974). Alkaline syenite dikes are localised in the endocontact zone of the complex and have secant contacts with jacupirangites and fenites (Fig. 2).

Geological study of the alkaline rocks of the Arbarastakh ultramafic carbonatite complex showed the specific geological sequence of alkaline phase crystallisation: jacupirangites and ijolites → carbonatites and phoscorites → dikes of alkaline syenites and alkaline ultramafic rocks. The petrographic, mineralogical and geochemical features of the carbonatites and phoscorites of the Arbarastakh complex, as well as the chemical compositions of the parental melts for these alkaline rocks, are described below.

3. Sample preparation and analytical methods

The samples used for mineralogical, melt and fluid inclusion investigations were collected during fieldwork on the Arbarastakh complex in 2019. Polished thin sections were prepared for petrographic investigations and polished rock samples were prepared for ore mineralogical analyses. These were studied in transmitted and reflected light, respectively, under a polarising microscope (Olympus BX51) equipped with a camera.

The polished rock samples were used to determine the rock textures and mineral assemblage compositions using energy-dispersive spectrometry in combination with back-scattered electron imaging (BSE) using a TESCAN MIRA 3 LMU JSM-6510LV scanning electron microscope (SEM) with the energy module from X-Max Oxford Instruments for microprobe analysis. Whole-rock compositions were determined by X-ray fluorescence (ARL-9900-XP).

Mineral compositions were determined using a JEOL JXA-8100 electron microprobe (WDS mode, 20 kV, 15nA, 1–2 μm beam diameter). The total time for analysing F (using an LDE crystal) was 40 s (background counting for 20 s, F peak counting for 20 s). The detection limit for F was 477 ppm (0.04 wt%). For mineral analysis, we used a beam current of 10nA and an acceleration voltage of 15 kV; for Fe–Ti oxides, we used 20nA and 15 kV; for monazite, we used 40nA and 20 kV; and for apatite, we used 10nA and 20 kV. The peak counting time was 16 s for major elements and 30–60 s for minor elements. For calibration, both natural minerals and synthetic phases were used as standards, with each element and detection limits in ppm reported in parentheses as follows: SiO_2 (Si, 158), rutile (Ti, 120), $LiNbO_3$ (Nb, 142), Sr silicate glass (Sr, 442), albite (Na, 176), orthoclase (K, 182), Al_2O_3 (Al, 128), F-apatite (Ca, 115; P, 387; F, 477), Mn-garnet (Mn, 129), hematite (Fe, 148), $CePO_4$ (Ce, 236), $LaPO_4$ (La, 272), $BaSO_4$ (S, 178), $NdPO_4$ (Nd, 362), Cl-apatite (Cl, 74) and $PrPO_4$ (Pr, 401).

Double-polished thin sections were prepared for melt and fluid inclusion investigations. Raman spectroscopy was applied to determine the crystalline phase compositions of the inclusions. Raman spectra were obtained on a LabRam HR800 Horiba Jobin Yvon spectrometer, equipped with an optical microscope (Olympus BX41). The 514.5 nm Ar+ laser line was used for spectral excitation. The well-known RRUFF (http://rruff.info) database was used to identify the solid phases. The polished preparations with open melt and fluid inclusions were also used for inclusion composition investigations under the SEM. Heating and freezing experiments were carried out using a TC-1500 heat chamber (Osorgin, 1990) with an inert atmosphere of purified argon and a Linkam THMSG-600 stage, and include the determination of homogenisation temperatures of inclusions.

The investigations were carried out at the Analytical Center for Multi-Elemental and Isotope Research Siberian Branch, Russian Academy of Science (Novosibirsk, Russia).

4. Results of investigations

4.1. Petrography and mineralogy of carbonatites and phoscorites

Petrography and mineralogy of the alkaline rocks of the Arbarastakh complex were previously described in the works of Glagolev et al. (1974) and Goroshko and Guryanov (2004), as well as in the reports of Russian geological prospecting expeditions. Below, we provide a summary of new investigations of the phase assemblages and mineral compositions of the carbonatites and phoscorites from the Arbarastakh complex.

The carbonatites are medium-grained rocks with a massive texture. A large number of varieties of carbonatites are present in the Arbarastakh complex: pyroxene-, phlogopite-, apatite-, pyrochlore-containing, etc. (Fig. 3 c – e). Varieties of carbonatites with feldspars, nepheline and fluorite are also found in the Arbarastakh complex (Fig. 4 a – h). The carbonatites of the Arbarastakh complex are mainly represented by calcite carbonatites (referred to simply as carbonatites below) and silicocarbonatites with SiO_2 ranging from 20 to 27 wt% (Le Maitre, 2002).

The mineral composition of carbonatites is represented by the primary minerals calcite (40–70%) and dolomite (10–20%), which make up to 50–90% of the rock volume, and varying amounts of phlogopite, clinopyroxene, apatite, amphibole, fluorite and feldspathoids (Fig. 4 a – h). The accessory and ore-bearing minerals (5–10%) include titanomagnetite, zircon, zirconolite, perovskite, pyrochlore, and baddeleyite. Ancylite-(Ce), bastnaesite-(Ce), burbankite, barite, strontianite, and rare sulphides such as chalcopyrite, pyrite and galena represent minor hydrothermal minerals (5–15%). Carbonatites may contain up to 5–10 vol % of K-feldspar nd/or nepheline, and 5–15 vol% of fluorite (Fig. 4 f, g).

The most common phoscorites are baddeleyite- and pyrochlore-containing ore varieties (Fig. 4 i – p). The ore-bearing rocks have a medium-grained structure and massive texture. The major minerals of the phoscorites include primary olivine, titanomagnetite, minerals of the spinel group, apatite, calcite and dolomite. The minor minerals are phlogopite, barite, barite–celestite, celestite, strontianite and barytocalcite with rare impregnations of sulphides such as chalcopyrite, pyrite and bismuthine. Accessory minerals in phoscorites are represented by baddeleyite and pyrochlore.

The investigated carbonatites and phoscorites of the Arbarastakh complex were formed during four paragenetic stages: magmatic, late-magmatic, hydrothermal-metasomatic, and hypergene (Fig. 5). The paragenetic scheme in Fig. 5 reflects the evolution of the main magmatic and ore-bearing accessory with Zr–Nb mineral assemblages to the hydrothermal and metasomatic stages with ore-bearing Ba–Sr–REE mineralisation, and then to the later stages of hypergene alteration of the alkaline rocks.

Mica is one of the main minerals in carbonatites and silicocarbonatites, and is represented by phlogopite and tetraferriphlogopite. The latter is typical for metasomatic altered carbonatites, while the mica of the phoscorites is more typically phlogopite (Fig. 4 a, b; Figs. 5 and 6; Table S1). The phlogopite forms euhedral leaves up to several cm in size; the crystals are zoned due to variations in the BaO/K_2O and FeO/MgO contents (Fig. 4 b). The chemical characteristics suggest that, during the crystallisation of the mineral, the FeO_t and Al_2O_3 concentrations tend to decrease while the MgO content increases (Table S1, Fig. 4 b; Fig. 6 a).

The trend of mica composition evolution is similar to other well-known phoscorite–carbonatite complexes worldwide (Fig. 6 b). The BaO content in the phlogopite can be enriched up to 4 wt%, and the TiO_2 is below detection limits (Table S1). The high BaO content in micas is typical for carbonatite–phoscorite complexes such as Palabora (Giebel et al. (2019) and carbonatites of the Belaya Zima complex (Doroshkevich et al., 2016). It is also typical for kimberlites (Mitchell, 1995) and ultramafic carbonatite complexes, such as olivinites of the Guli massif from the Maymecha–Kotuy province or aillikites from the

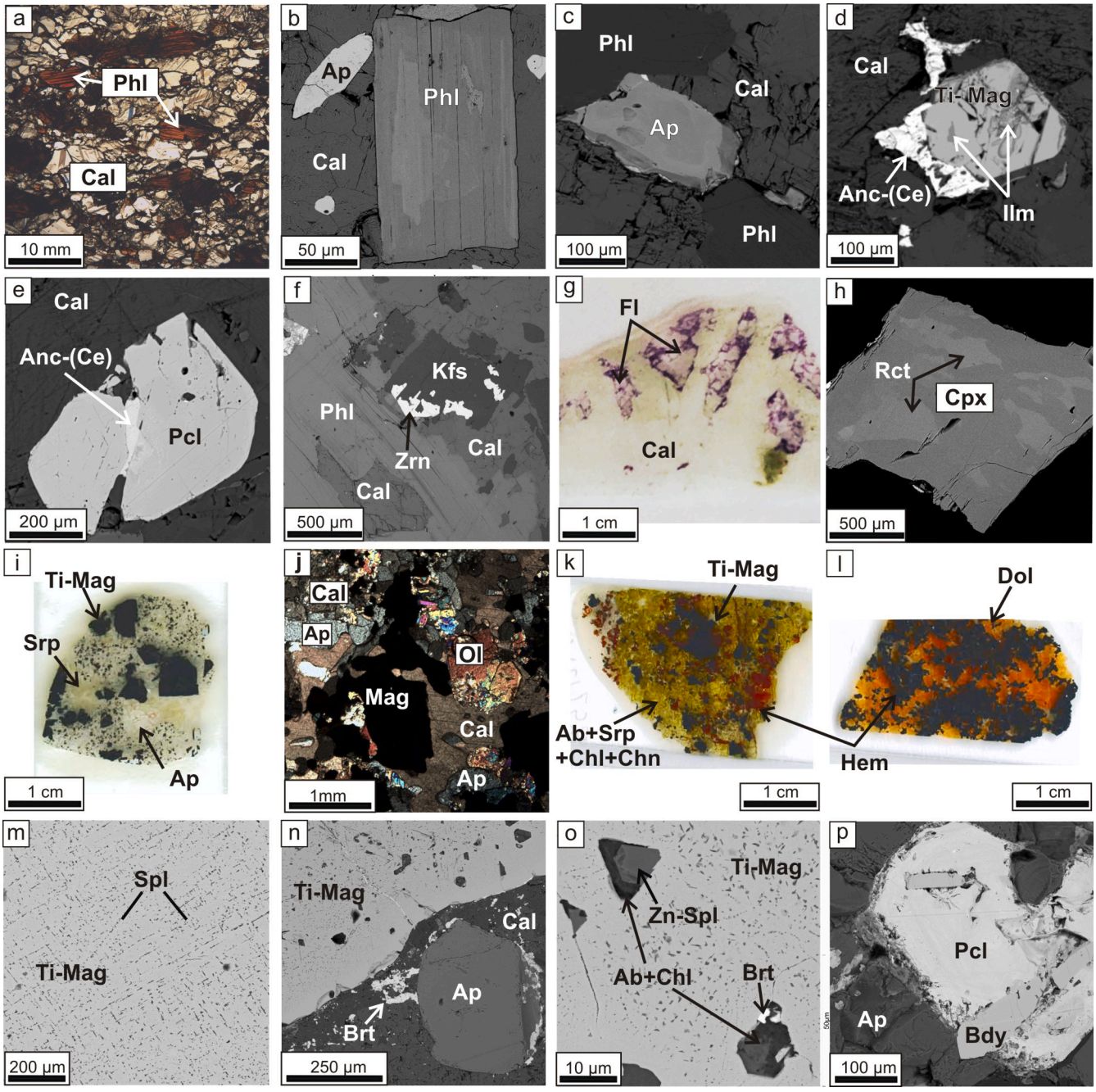

Fig. 4. Mineral assemblages of carbonatites (a – h) and phoscorites (i – p) from the Arbarastakh complex: petrographic photographs (a, j), BSE images (b – f, h, m – p) and thin section photographs (i, k, l). Mineral abbreviations are taken from Whitney and Evans (2010). Carbonatites consist of calcite matrix with zoned phlogopite and fluorapatite crystals (a – c). Ti-magnetite crystals are rare and contain ilmenite inclusions; hydrothermal mineralisation includes REE-carbonates such as bastnaesite-(Ce) and ancylite-(Ce) (d). Accessory pyrochlore with hydrothermal ancylite-(Ce) in calcite matrix (e). Carbonates also include K-feldspar and/or nepheline (f), and fluorite (g); clinopyroxene in silicocarbonatites is replaced by richterite (h). Phoscorites are composed of Ti-magnetite and olivine crystals in a carbonate (calcite and dolomite) matrix with apatite grains (i, j). Hydrothermal–metasomatic assemblages present serpentine, albite, chlorite, chondrodite, carbonates (dolomite and siderite), barite and hematite (k, l) as secondary minerals. Ti-magnetite includes the spinel-group minerals as a product of solid solution decay; the inclusions were subjected to hydrothermal-metasomatic alteration with formation of the Zn-spinel, chlorite and albite assemblages, as well as barite, celestite and strontianite granular aggregates (m – o). Accessory Nb-minerals of the phoscorites form the baddeleyite–pyrochlore banded subhedral crystal aggregates (p).

Chadobets complex (Prokopyev et al., 2020), and for the metasomatised mantle xenoliths of eastern Antarctica (Kogarko et al., 2007, 2012).

Apatite in the carbonatites and phoscorites is represented by fluorapatite and contains up to 2 wt% F, up to 0.6% light REEs (LREE) in the form of $LREE_2O_3$, up to 0.2% Na_2O and up to 0.8% SrO (Table S2). Fluorapatite forms prismatic idiomorphic crystals from 0.1 to 1 cm in size in the carbonatites (Fig. 4 c). Sometimes, fluorapatite forms euhedral grains and assemblages with magmatic dolomite and pyrochlore (Fig. 4 e). The fluorapatite in the phoscorites occurs as euhedral and subhedral grains up to several cm in size, crystallising after olivine and magnetite crystals (Fig. 4 i, j, n). Fluorapatite in the carbonatites forms zoned crystals because of the increasing LREE contents from the centre to the edge of the crystals (Fig. 4 c; Table S2), which indicates the removal of REEs from the fluorapatite due to late hydrothermal-metasomatic processes (e.g. Hogarth, 1989; Harlov and Förster, 2004; Broom-Fendley et al., 2016; Chakhmouradian et al., 2017; Prokopyev

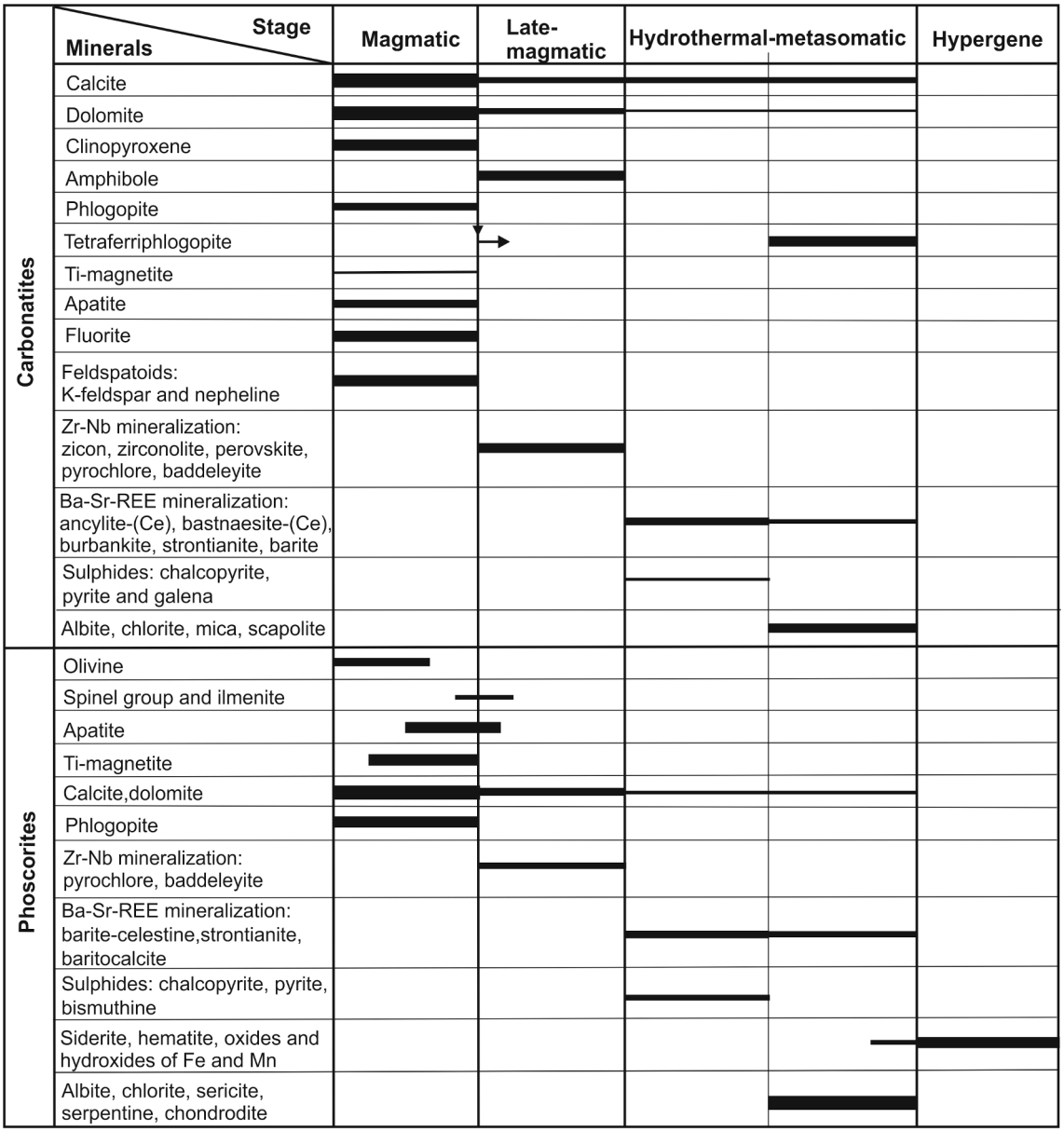

Fig. 5. Paragenetic scheme of the mineral assemblages of carbonatite and phoscorite formation from the Arbarastakh alkaline complex.

et al., 2017).

Magnetite forms idiomorphic grains in carbonatites up to 1 mm in size, and belongs to the titanomagnetite group (Fig. 4 d; Fig. 5). The crystals consist of up to 0.6 wt% TiO_2 and contain ilmenite inclusions (Table S3). The titanomagnetite in phoscorites occurs as idiomorphic grains and aggregates up to 1 cm in size (Fig. 4 i – o). It includes inclusions of the *spinel-group minerals* and *ilmenite*. The spinel inclusions have octahedral and rhombohedral sections or ellipsoidal shapes; they lie along the crystallographic directions of the magnetite crystals, which indicates that the spinel phases were formed due to solid solution decay (Fig. 4 m – o). The size of the inclusions ranges from 5 to 20 μm. The spinel-group minerals in the carbonatites are represented by magnetite and ulvospinel end-members with jacobsite content (Table S3). The phoscorites contain spinels with small contents of jacobsite, magnesioferrite and gahnite (Table S3). Mineral phases of Zn-spinel and ilmenite were also found in the phoscorites of the Kovdor carbonatite complex (Wall and Zaitsev, 2004).

Clinopyroxene forms idiomorphic grains up to several cm in size and is predominantly crystallised in the silicocarbonatites (Fig. 4 h; Fig. 5). The clinopyroxenes include melt inclusions. The mineral belongs to the diopside–hedenbergite–aegirine composition with small concentrations of jadeite and alumino-tschermacite end-members (Table S4, Fig. 7). The composition of the clinopyroxene differs slightly from the carbonatites of the Belaya Zima alkaline complex (Doroshkevich et al., 2017) and corresponds to the buffer $\Delta FMQ = +1$ to $+2$ as a qualitative indicator of oxygen fugacity in the mineral system (Fig. 7).

Amphibole in the silicocarbonatites of the Arbarastakh complex presents as richterite (Fig. 7 b), which replaces the clinopyroxene crystals (Fig. 4 h; Fig. 5). The richterite mineral phases were also found in the crystal–fluid inclusions in diopside from the silicocarbonatites (*Section 4.2*).

The pyrochlore group minerals are the main concentrators of niobium and uranium in the phoscorites and carbonatites (Table S5); they form octahedral crystals up to 1 cm in size (Fig. 3 d; Fig. 4 e, p). In the phoscorites, the Nb-minerals form the baddeleyite–pyrochlore banded subhedral crystal aggregates (Fig. 4 p; Fig. 5).

Baddeleyite and *zircon* are quite rare in carbonatites (less than 1 vol %) and usually occur in the phoscorites, forming subhedral elongated

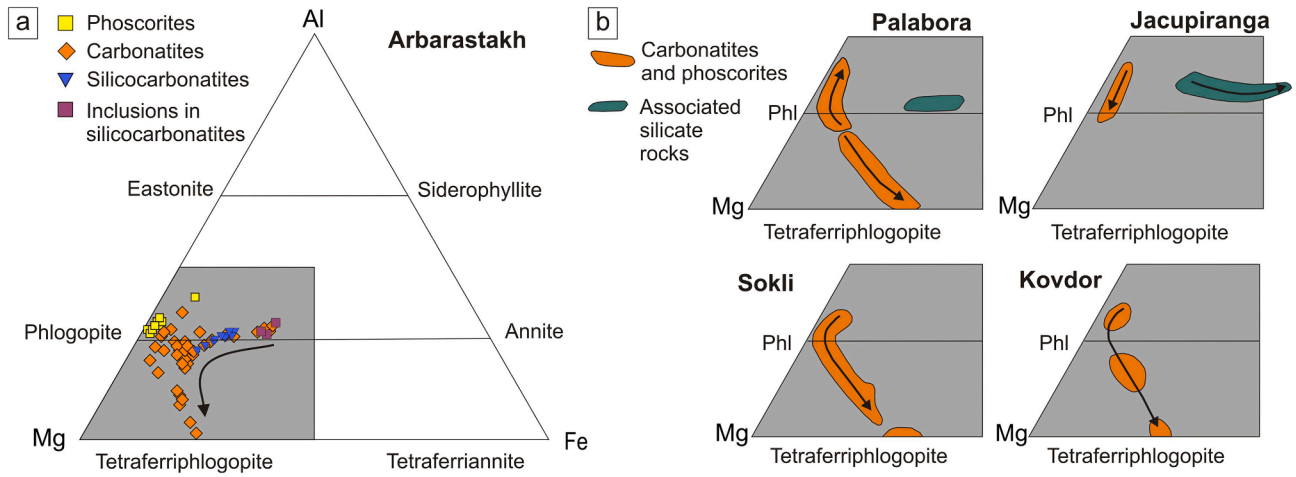

Fig. 6. Composition of mica for the carbonatites and phoscorites from the Arbarastakh alkaline complex according to Mitchell (1995) (a). Compositional trends of mica from Palabora (Giebel et al., 2019), Jacupiranga (Brod et al., 2001), Sokly (Lee et al., 2003), and Kovdor (Krasnova et al., 2004a) carbonatite–phoscorite complexes (b).

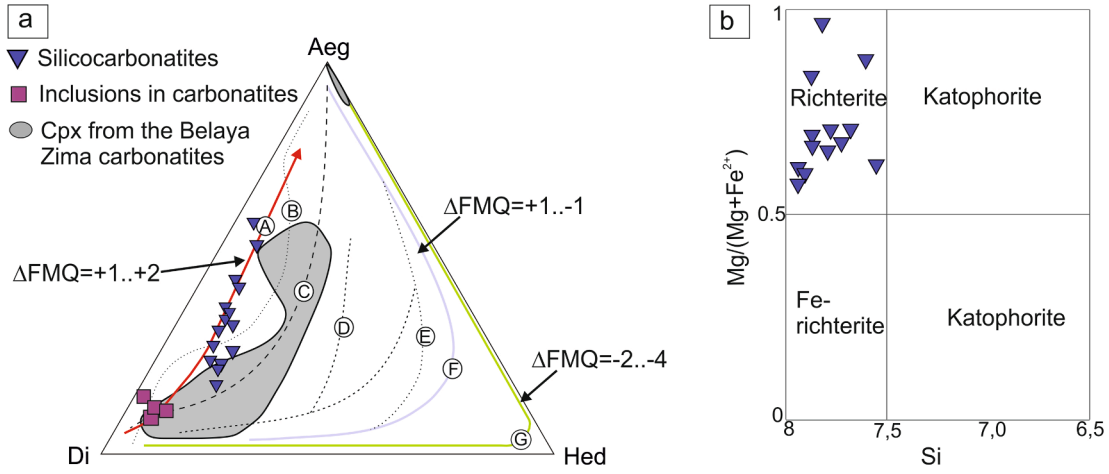

Fig. 7. Composition of clinopyroxenes in carbonatites from the Arbarastakh complex, and clinopyroxene evolution trends from various alkaline complexes worldwide (Mann et al., 2006) (a): Katzenbuckel, SW Germany (A); Murun, Russia (B); Lovozero, Russia (C); Alnö, Sweden (D); Coldwell nepheline syenites, Canada (E); North Qôroq, South Greenland (F); Ilímaussaq, South Greenland (G). The clinopyroxene composition of the carbonatites from the Belaya Zima complex was taken from Doroshkevich et al. (2017). Quantitative data on oxygen fugacity (given as ΔFMQ units, where FMQ is the fayalite–magnetite–quartz buffer) imply that the chemical evolution of clinopyroxene might be useful as a qualitative indicator of oxygen fugacity. Classification of analysed amphiboles in Si versus $Mg/(Mg + Fe^{2+})$ (apfu) diagram (b) (after Leake et al., 1997).

and prismatic crystals; the content of HfO_2 in the baddeleyite is up to 1.8 wt%. These minerals form in the late-magmatic stage (Fig. 5).

Olivine in the phoscorites forms subhedral and idiomorphic crystals of up to several cm in size (Fig. 4 j; Fig. 5). The Fo content of the olivines is 65–68%. Olivine is intensively replaced by secondary serpentine and chondrodite.

The *feldspars and feldspathoids* are represented by magmatic K-feldspar and nepheline, as well as metasomatic albite (Fig. 4 f, k; Fig. 5). The minerals usually form idiomorphic crystals in the carbonate matrix. K-feldspar is orthoclase (Or_{85-100}) with small amounts of CaO and Na_2O (up to 0.5 wt%). The mineral composition of plagioclase contains up to 1 wt% of CaO and a small amount—up to 0.45 wt%—of K_2O; nepheline is intensively replaced by scapolite.

Fluorite in the carbonatites forms cubic crystals and aggregates up to several cm in size, and includes up to 0.35 wt% Y_2O_3 as shown by SEM (Fig. 4 g; Fig. 5).

Primary *carbonates* of the phoscorites and carbonatites are represented by calcite and dolomite (Figs. 4 and 5). The minerals form prismatic crystals ranging in size from 0.1 to 5 mm and contain up to 1.6 wt % SrO; BaO is present up to 0.98 wt% in dolomite (Table S6.1). Hydrothermal carbonates form veins and secondary aggregates of dolomite, strontianite and siderite with hydrothermal mineral assemblages (Fig. 5). The SrO content of the hydrothermal carbonates is below the detection limit.

Hydrothermal minerals are represented by assemblages of *barite, barite–celestite, ancylite-(Ce), bastnaesite-(Ce), and burbankite*, forming microveins and aggregates in the carbonates, or crystallising along the periphery of apatite and magnetite crystals (Fig. 4 d, n, o; Fig. 5). Representative analyses of the hydrothermal REE-carbonates, barite and strontianite from the carbonatites are provided in Table S7, and the chemical compositions of Ba–Sr sulphates and strontianite in the phoscorites are given in Table S8. The strontianite includes up to 1.7 wt% BaO, and up to 10.7 wt% CaO. The barite–celestite minerals contain up to 10.8 wt% CaO. Burbankite shows strong variation in Na, Sr, Ba and REEs.

The studied carbonatites and phoscorites were subjected to intense hydrothermal-metasomatic processes with formation of ore-bearing metasomatites with mineral assemblages of *chlorite, sericite, albite,*

serpentine, chondrodite, secondary carbonates *dolomite and siderite, hematite, and oxides and hydroxides of Fe and Mn* (Figs. 4 and 5). Minor hydrothermal minerals also include rare micro-impregnations and veins of sulphides such as *chalcopyrite, pyrite and galena*, which are located in the metasomatic rocks. The chalcopyrite phases were determined in the melt inclusions; their composition suggests that the chalcopyrite could be also magmatic (see next section).

4.2. Melt and fluid inclusion study

4.2.1. Carbonatites and silicocarbonatites

Melt, polycrystalline and crystal–fluid inclusions were identified in the phlogopite, clinopyroxene and albite from the carbonatites and silicocarbonatites (Fig. 8). This is the first data describing the melt and fluid inclusions of the Arbarastakh alkaline complex.

The melt inclusions in phlogopite and clinopyroxene of the carbonatites are primary fluid inclusions (Roedder, 1984); they are located in the central parts of the matrix and usually have a round shape or negative crystal shape, 10–20 μm in size (Fig. 8 a – d). SEM analyses of

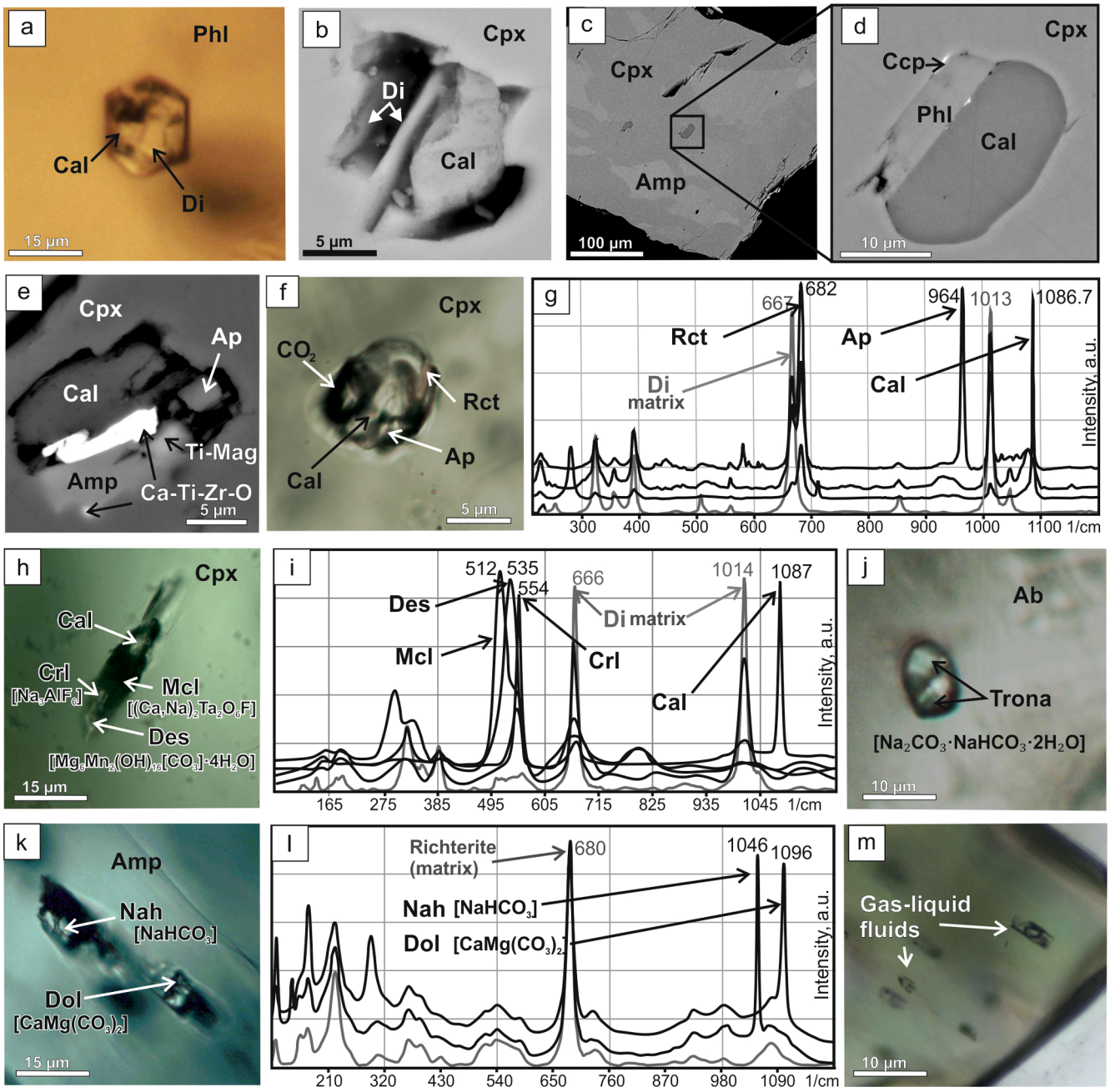

Fig. 8. Inclusions in the minerals of the Arbarastakh complex carbonatites. Micro-photograph of the primary melt inclusion in phlogopite (a). BSE image and composition of an opened melt inclusion in a clinopyroxene (b) from the carbonatites; BSE images of location (c) and composition (d) of an opened melt inclusion in a clinopyroxene of the silicocarbonatites. BSE image and composition of the opened crystal–fluid inclusions in the clinopyroxene (e), micro-photograph and composition of the crystal–fluid inclusions (f, h, k) and Raman spectra of the daughter phases of the inclusions (g, i, l) in diopside and amphibole (Mcl – fluorcalciomicrolite, Des – desautelsite, Crl – cryolite, Nah – nahcolite). Micro-photograph of a polycrystalline inclusion in albite with trona mineral phases (j), and micro-photograph (m) of late gas–liquid fluid inclusions in the clinopyroxene.

opened melt inclusions in the carbonatites revealed the presence of calcite and diopside daughter phases (Fig. 8 a, b). The chemical composition of the clinopyroxene daughter phases differs from the matrix by its relatively higher diopside content (Table S4; Fig. 7).

SEM analyses of opened melt inclusions in clinopyroxene from the silicocarbonatites showed the presence of phlogopite and calcite daughter phases, as well as chalcopyrite phases (Fig. 8 c, d). The daughter phases of phlogopite have higher FeOt and lower MgO contents in comparison with phlogopite from the silicocarbonatites (Table S1; Fig. 6 a). Variations in the composition of mica in carbonatites overlap the composition field of phlogopites in the silicocarbonatites and daughter phases of inclusions, while the composition of phlogopite in the phoscorites is characterised by a relatively sharp decrease in the FeO_t content (Fig. 6 a). The composition of the calcite daughter phase is similar to the composition of the calcite mineral phase in the carbonatites (Tables S6.1, S6.2).

The primary crystal–fluid inclusions in the clinopyroxenes of carbonatites are between 10 and 25 μm, and consist predominantly of carbonate calcite daughter phases (60–70 vol%), with up to 10–25 vol% richterite, apatite, Ti-magnetite and complex Ca–Ti–Zr oxide ore phases also present (Fig. 8 e – g). The fluid phase of the inclusions contains liquid CO_2 according to Raman spectroscopy (Fig. 8 f). We could not

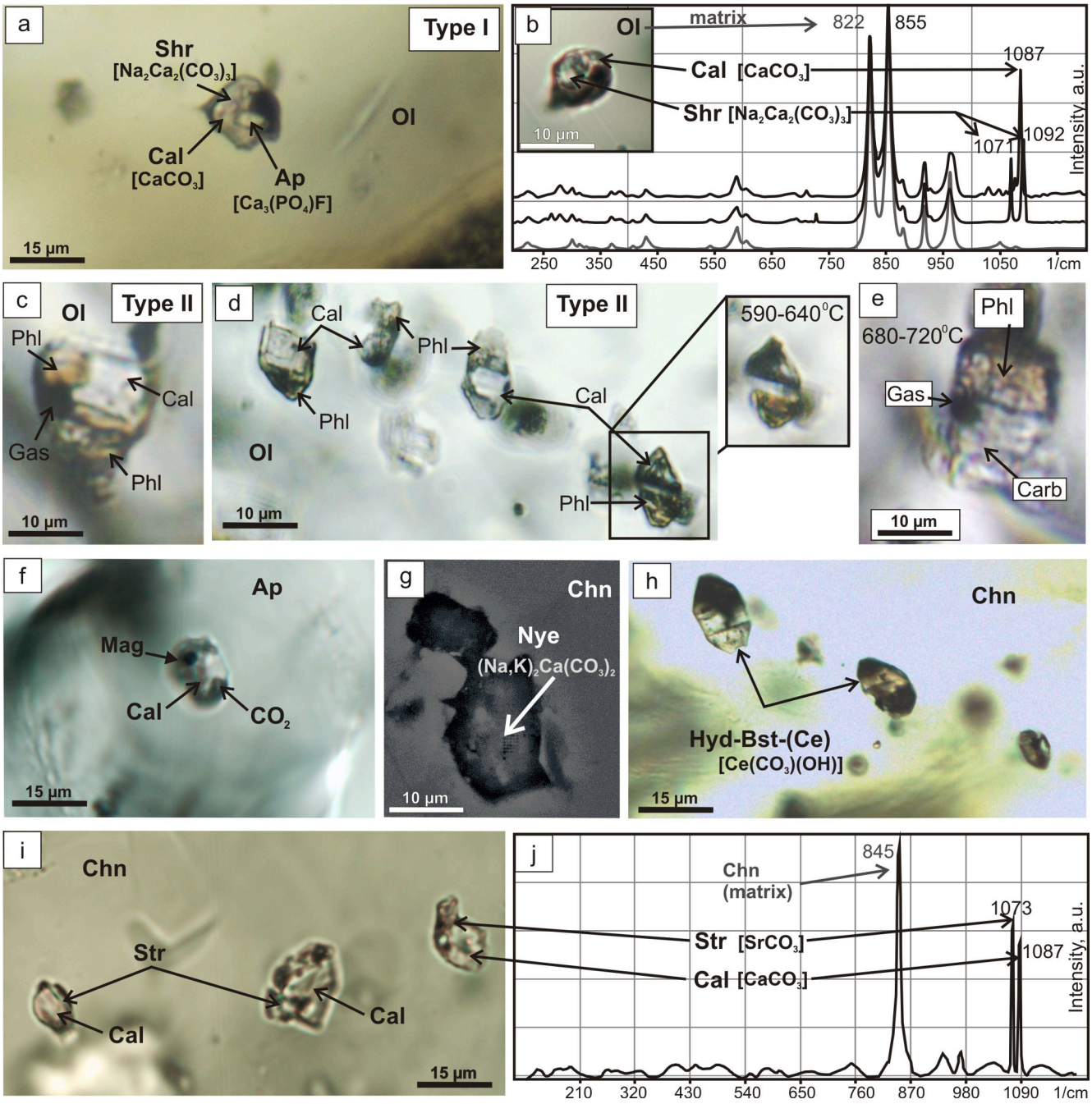

Fig. 9. Inclusions in the minerals of the phoscorites of the Arbarastakh complex. Micro-photograph and composition of the secondary melt inclusions (type I) in olivine (a), Raman spectra of the daughter phases of the inclusion (type I) (Shr – shortite) (b); micro-photograph and composition of the secondary melt inclusions (type II) in olivine (c – e), with photographs of the heated inclusions during the thermometric experiments. Photograph and composition of a primary melt inclusion in apatite (f). BSE image of an inclusion with nyerereite (Nye) mineral phase (g), and micro-photographs and composition of secondary crystal–fluid inclusions (h, i) in chondrodite; the Raman spectra (j) of the daughter phases of the inclusions (i).

determine the true homogenisation temperature of the highly concentrated crystal–fluid inclusions due to the presence of xenogenic phases, but partial homogenisation (dissolution of the fluid phase) was estimated to occur at 540–575 °C. Homogenisation of CO_2 into the liquid phase occurs at +10.1 to +11.8 °C, which corresponds to a density of 0.85–0.86 g/cm^3. Using the obtained inclusion homogenisation temperatures, the minimum pressure of the fluid inclusion capture was estimated to be 2.9–3.3 GPa using the FLINCOR program (Brown, 1989).

The clinopyroxenes of the carbonatites also include secondary crystal–fluid inclusions, consisting of the crystal phases of fluorcalciomicrolite [$(Ca,Na)_2(Ta)_2O_6F$], desautelsite [$Mg_6Mn_2(OH)_{16}[CO_3]\cdot 4H_2O$] and cryolite [$Na_3AlF_6$], determined by Raman spectroscopy (Fig. 8 h, i). The temperature of homogenisation (dissolution of the crystal phases) of the inclusions was estimated to be 300–350 °C. The polycrystalline and crystal–fluid inclusions were found in the metasomatic albite and secondary richterite (Fig. 8 j – l). The polycrystalline inclusions in the albite crystals contain trona minerals [$Na_2CO_2\cdot NaHCO_2\cdot 2H_2O$], which probably crystallised as alteration products of the alkali carbonates (Fig. 8 j). The crystal–fluid inclusions in the richterite of the silicocarbonatites consist of nahcolite [$NaHCO_3$] and dolomite daughter phases, according to the Raman spectroscopy data (Fig. 8 k, l). The fluids trace late hydrothermal processes, and homogenised at 250–280 °C.

Carbonatite and silicocarbonatite minerals (e.g. phlogopite, calcite, clinopyroxene and amphibole) as well as phoscorites also contain a large number of secondary gas–liquid fluid inclusions tracing the late hydrothermal and metasomatic processes (Fig. 8 m). These inclusions have rounded and irregular shapes, contain CO_2 in the gas phase, and vary in size from 5 to 15 μm. The concentration of such fluids was estimated as 5–15 wt% NaCl-equ., according to the eutectic temperatures of −11 to −5 °C (Roedder, 1984). The homogenisation temperature of the gas–liquid fluid inclusions falls within the range 150–300 °C.

4.2.2. Inclusions in phoscorites

Olivine crystals in the phoscorites contain two types of secondary melt inclusions, which differ by location, inclusion vacuole forms and mineral phases compositions within the inclusions (Fig. 9 a – d). Type I melt inclusions have round shapes and are located along the planes of crystal growth and in certain orientations (Fig. 9 a, b); their sizes range from 5 to 15 μm, and the daughter phases are represented by apatite and by carbonates, predominantly calcite and shortite [$Na_2Ca_2(CO_3)_3$], according to the Raman spectroscopy data (Fig. 9 a, b). Type I melt inclusions contain gas bubbles (2–5 vol%), and their homogenisation temperatures are estimated as 680–720 °C.

Type II secondary melt inclusions in the olivine crystals are found at healed fractures and planes of the matrix (Fig. 9 c, d); the inclusions usually have a negative crystal shape, and range in size from 10 to 15 μm. These melt inclusions consist of polycrystalline aggregates of the phlogopite and calcite daughter phases, with gas bubble phases (Fig. 9 c, d); the melt inclusion silicate and carbonate volume contents are roughly equal. When the melt inclusions were heated, melting of the silicate and carbonate phases began at 590–640 °C (Fig. 9 d), and at the temperature range of 680–720 °C the melt inclusions were decrepitated (Fig. 9 e).

Melt inclusions were also identified in the fluorapatite grains of the phoscorites (Fig. 9 f). The inclusions are located singly or grouped in the central parts of the matrix, and could be attributed to primary capture. The melt inclusions are approximately 15 μm in size; they are composed predominantly of calcite daughter phases, with Ti-magnetite phases, and contain CO_2 in the gas phase (Fig. 9f). The homogenisation temperature of the melt inclusions is similar to that of the type I melt inclusions, occurring at 680–700 °C.

Chondrodite (replacing the olivine) of the phoscorites contains mineral and crystal–fluid inclusions of about 10–15 μm in size (Fig. 9 g – j). The mineral inclusions are irregularly-shaped and contain the mineral phase nyerereite [$(Na,K)_2Ca(CO_3)_2$] (Fig. 9 g), which contains up to 0.5 wt% K_2O according to the SEM analyses. The highly concentrated crystal–fluid inclusions in the chondrodite are secondary and are located along fractures and planes. The inclusions represent two generations: inclusions containing hydroxyl-bastnaesite-(Ce) [$Ce(CO_3)(OH)$] crystalline phases (Fig. 9 h), and carbonate fluid inclusions with strontianite and calcite daughter phases, determined by Raman spectroscopy (Fig. 9 i, j). The crystal–fluid inclusions with calcite and strontianite salt phases have homogenisation temperatures in the range of 480–500 °C, while the secondary fluids with hydroxyl-bastnaesite-(Ce) phases were homogenised at 430–450 °C. The fluid inclusions were homogenised into the liquids, and were most likely responsible for the formation of the Ba–Sr–REE hydrothermal mineralisation of the ore-bearing phoscorites.

5. Discussion

5.1. Model of the formation of the Arbarastakh complex

The Neoproterozoic epoch (725–630 Ma) of intraplate alkaline magmatism manifesting on the Siberian Craton is represented by a large group of rare-metal alkaline ultramafic carbonatite complexes, associated with superplume activity and structurally inclining towards the marginal parts of the craton (Yarmolyuk et al., 2005; Fig. 1). Examples of such complexes include Belaya Zima, Tagna, Zhidoy, Ingili and the Arbarastakh carbonatite-phoscorite complex, located along the southwestern boundary of the craton from the Sharyzhalgay uplift to the Aldan Shield, within the marginal fault system zones of the Siberian Craton (Yarmolyuk et al., 2005; Kuzmin and Yarmolyuk, 2014). The similar timing of the formation of these alkaline complexes is consistent with the epoch of large-scale manifestation of intraplate magmatism in the Siberian Craton. This group of alkaline rocks and associated carbonatites are almost certainly linked with 720 Ma Irkutsk Large Igneous Province (LIP) that is reconstructed with the coeval Franklin LIP of northern Laurentia (Ernst et al., 2016). The history of the formation of these alkaline ultramafic complexes is directly related to geodynamic events of the period of 700–600 million years ago, which reflected the disintegration of the supercontinent Rodinia (e.g. Yarmolyuk et al., 2005; Kuzmin and Yarmolyuk, 2014).

The origin of the carbonatitic melts is related to mantle processes such as carbonate metasomatism of peridotite, which occurs at estimated depths of ~180–250 km under the Siberian Craton (Fig. 10 a) (e.g. Mitchell, 1995; Kogarko et al., 1997; Tappe et al., 2005, 2006; Andreeva et al., 2007; Doroshkevich et al., 2017, 2019; Nosova et al., 2018, 2020; Prokopyev et al., 2020). The interpretation of aeromagnetic and gravimetric data allows us to consider the Arbarastakh complex as a pipe-like body, with a portion expanding downward at a depth of about 8–10 km (Goroshko and Guryanov, 2004), which could be assumed to be the position of an intermediate chamber. In addition, these data are consistent with the 2.9–3.3 GPa estimates of the capture pressure of the orthomagmatic fluid inclusions. The intermediate chamber is a possible site for the carbonatite primary melt evolution and the parental melt origin of the associated jacupirangites (Fig. 10 a, b). Mineralogy and melt inclusion investigations show that the silicocarbonatites and carbonatites of the Arbarastakh complex were crystallised from a silicate–carbonate alkaline melt with high Ca, K and Na contents (predominantly calcite, phlogopite and diopside mineral and daughter phases) (Fig. 10 a, b). The mechanism and temperatures of formation of the primary melts for the Arbarastakh carbonatites could be determined according to the study of melt inclusions in the associated alkaline silicate rocks (i.e. jacupirangites). Andreeva et al. (2007) and Andreeva (2014) provided evidence from melt inclusion studies for the contributions of crystallisation differentiation and silicate–carbonate liquid immiscibility to the ijolites and carbonatites of the Belaya Zima ore-bearing alkaline complex. However, the petrological investigations of the Belaya Zima alkaline rocks revealed the gradual increase of Zr, Nb and REE concentrations in the magma, which is consistent with the

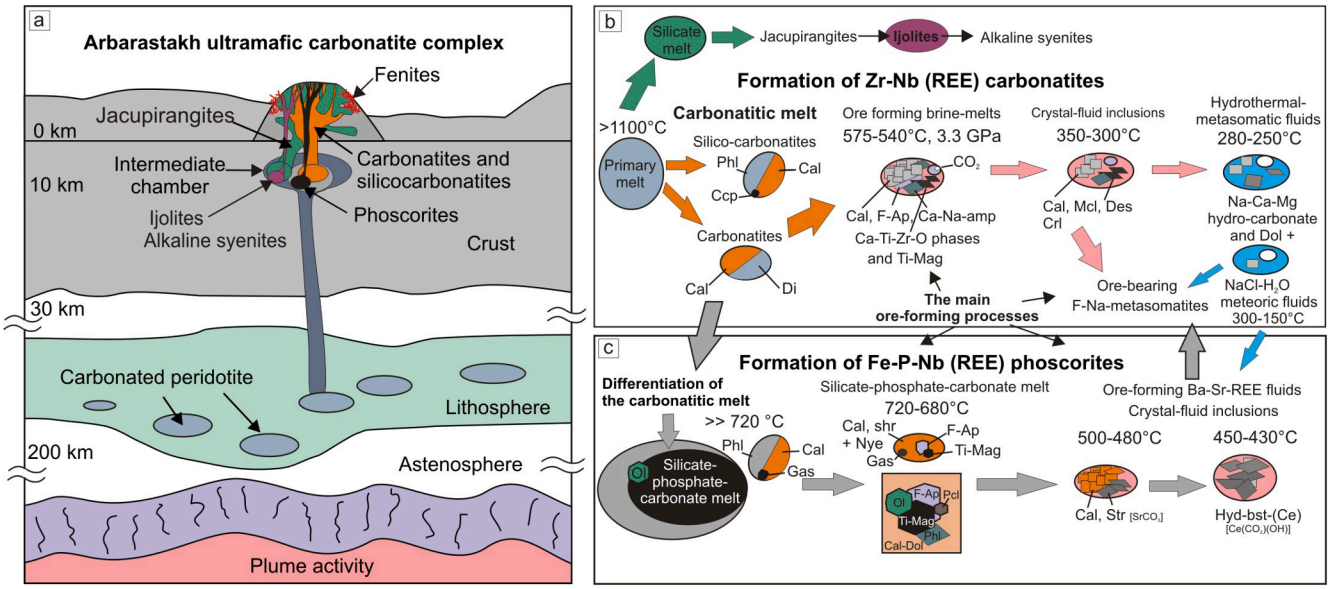

Fig. 10. Schematic model of formation of the ore-bearing carbonatites and phoscorites of the Arbarastakh complex (see description in the text).

process of extensive fractional crystallisation and a gradual transition from silicate rocks to carbonatites (Doroshkevich et al., 2017). We can preliminarily assume a temperature of more than 1100 °C for the primary melt generation of the Arbarastakh rocks, as was determined for the associated silicate rocks of the Belaya Zima carbonatite complex (Andreeva et al., 2007).

The phlogopite composition of the daughter phases in the melt inclusions of the Arbarastakh silicocarbonatites lies at the beginning of the evolutionary trend for the carbonatite and silicocarbonatite micas (Fig. 6 a). The evolutionary trend from the phlogopite to tetraferriphlogopite has been described for many carbonatite–phoscorite complexes (Fig. 6 b), e.g. Kovdor and Sokli (Rimskaya-Korsakova and Sokolova, 1964; Lee et al., 2003; Krasnova et al., 2004a), Palabora (Giebel et al., 2019) and Jacupiranga (Brod et al., 2001). The trend reflects the metasomatic alteration of the carbonatites (e.g. Brod et al., 2001), and the tetraferriphlogopite crystallisation is caused by the low availability of Al combined with a high fO_2 (Brigatti et al., 1996; McCormick and Le Bas, 1996; Lee et al., 2003).

The chemical composition of mica in the Arbarastakh alkaline rocks indicates that the carbonatites and silicocarbonatites were formed in multiple stages, while the phoscorites were crystallised from the differentiated carbonatitic melt with decreased FeO_t content (Fig. 6 a). The carbonatite and silicocarbonatite micas produce different trends from a single source, and trend in the same direction, while significant compositional variations and the character of the transition from phlogopite to tetraferriphlogopite indicate that the carbonatites are more differentiated than the silicocarbonatites and most likely formed later.

The clinopyroxene composition in the silicocarbonatites of the Arbarastakh complex shows a sharp transition from diopside to aegirine that confirms the high fO_2 during crystallisation of the mineral (ΔFMQ = +1 to +2; Fig. 7 a), and the composition of clinopyroxene from the melt inclusions in carbonatites is located at the beginning of the trend (Fig. 7 a). For the fluids accompanying the formation of picrite melts of the Maimecha-Kotuy alkaline province, the ΔFMQ values are +2 to +2.5 (Ryabchikov et al., 2002), and transformations of the mantle rocks are carried out by alkaline carbonate-containing fluids characterised by ΔFMQ values of −0.76 to −0.06 (Kogarko, 2005). The ΔFMQ data for the Arbarastakh complex fall between the estimated values and differ slightly from the Belaya Zima carbonatites (Fig. 7 a).

The accessory ore-bearing Zr–Nb mineralisation of the Arbarastakh carbonatites was formed at the late-magmatic stage and consists of zircon, zirconolite, perovskite, pyrochlore and baddeleyite (Fig. 5). According to the crystal–fluid inclusion measurements, the active silicate–phosphate–carbonate melts took part in the process of forming the Zr–Nb mineralisation of the carbonatites (Fig. 10 b); the orthomagmatic fluids were generated at temperatures of more than 540–575 °C. The melts are characterised by high Ca, Na, F, P and Fe contents according to the composition of the crystal–fluid inclusions, and contain REEs (i.e. REE-fluorapatite daughter phase) (Fig. 10 b). The orthomagmatic brine melts could be responsible for the fluorite and carbonate hydrothermal mineralisation, for the removal of the LREE from the fluorapatite (e.g. Hogarth, 1989; Broom-Fendley et al., 2016; Chakhmouradian et al., 2017; Prokopyev et al., 2017) and the formation of the ore-bearing REE-hydrothermal mineralisation with ancylite-(Ce), bastnaesite-(Ce) and burbankite (Fig. 5).

The orthocarbonatitic fluids evolved to saline (60–70 wt%) crystal–fluids of Na–Ca–Mg–F–carbonate composition at more than 350–300 °C; later, the Na–Ca–Mg–hydro–carbonate fluids originated at temperatures of more than 280–250 °C, which evolved to fluids of NaCl–H_2O composition at a temperature range of about 300–150 °C (Fig. 10 b). The hydrothermal Na–Ca–F–carbonate/hydro–carbonate fluids are responsible for the Na–F metasomatic processes and formation of albitites with complex orthomagmatic (Zr–Nb) and hydrothermal (F-REE) ore mineralisation of the Arbarastakh carbonatites (Fig. 10 b).

The mineralogy (e.g. phlogopite composition) and melt inclusions of the phoscorites of the Arbarastakh complex revealed that the rocks were formed from a differentiated carbonatitic melt of silicate–phosphate–carbonate composition at a temperature much higher than 720 °C (Fig. 10 c). The crystallisation of minerals in the phoscorites proceeded as follows: olivine, Ti-magnetite, F-apatite, phlogopite and pyrochlore in the carbonate matrix (Fig. 10 c). The olivine crystals crystallised first (as the liquidus mineral), and in the process of crystallisation they captured evidence of the differentiated silicate-carbonate melts in the form of melt inclusions (for example, inclusions with phlogopite–calcite daughter phases, which are similar to melt inclusions in the silicocarbonatites), as well as the products of the parental melt evolution to the Fe–phosphate–carbonate melt (e.g. nyerereite inclusions, calcite, shortite, fluorapatite and Ti-magnetite daughter phase compositions of the melt inclusions) (Fig. 10 c).

The ore-bearing Fe–P–Nb phoscorites were subjected to the activity of ore-forming orthomagmatic fluids with Ca–Sr–carbonate and REE–hydro–carbonate compositions at temperature ranges of more than 480–500 and 430–450 °C, respectively. The fluids were responsible for

the hydrothermal Ba–Sr–REE mineralisation of barite, barite–celestite, celestite, strontianite and barytocalcite with hydroxyl-bastnaesite (Fig. 10 c). The saline (~50–70 wt%) fluids traced the formation of the ore-bearing F–Na–metasomatites in the carbonatites of the Arbarastakh carbonatite–phoscorite complex (Fig. 10 b, c).

The Na–Ca–carbonatite complexes of the Siberian Craton margin (Tagna and Belaya Zima) differ from the Arbarastakh complex by the absence of phoscorites. Research on the mechanisms of formation of well-known phoscorite complexes such as Kovdor (Russia) and Palabora (South Africa) show that both crystal fractionation and liquid immiscibility seem able to cause phoscorite generation (e.g. Rimskaya-Korsakova and Krasnova, 2002; Giebel et al., 2019; Rass et al., 2020). The fractional evolution of the carbonatitic melt from the phoscorites to the carbonatites was described for the Guli alkaline complex on the Siberian Craton (Russia) (Kogarko et al., 1997). The phoscorites of the Salitre I carbonatite complex (Brazil) were formed from different magma sources and through distinct processes due to fractional crystallisation and by means of melt immiscibility (Barbosa et al., 2020). Currently, we have determined the relationship between the petrogenesis processes for the phoscorites and carbonatites of the Arbarastakh alkaline complex, and we plan to clarify the formation mechanisms of the alkaline silicate and carbonate rocks in further studies.

6. Conclusions

1. Carbonatites of the Arbarastakh complex are represented by calcite carbonatites and silicocarbonatites. The rocks include primary calcite and dolomite with varying amounts of phlogopite, clinopyroxene, fluorapatite, amphibole, fluorite, K-feldspar and feldspathoids. The ore-bearing Zr–Nb mineral assemblages include zircon, zirconolite, perovskite, pyrochlore and baddeleyite. The Ba–Sr–REE hydrothermal mineralisation consists of ancylite-(Ce), bastnaesite-(Ce) and burbankite, as well as barite and strontianite.
2. The principal magmatic minerals of the phoscorites are represented by olivine (forsterite), Ti-magnetite, apatite, calcite and dolomite, as well as minor minerals of the spinel group and phlogopite. The Nb–Zr mineralisation includes baddeleyite and pyrochlore. Ba–Sr–REE minerals include barite, barite–celestite, celestite, strontianite, barytocalcite, and hydroxyl-bastnaesite-(Ce).
3. The silicocarbonatites and carbonatites of the Arbarastakh complex were crystallised in multiple stages from a silicate–carbonate alkaline melt with high Ca, K and Na contents. The phoscorites are the products of differentiation of the carbonatitic melt.
4. The silicate–phosphate–carbonate melts took part in the formation of the ore-bearing Zr–Nb mineralisation of the carbonatites at temperatures of more than 575–540 °C; saline (60–70 wt%) crystal–fluids of Na–Ca–Mg–F–carbonate composition at ~350–300 °C were responsible for the hydrothermal ore-bearing Ba–Sr–REE mineralisation. The ore-bearing Fe–P–Nb phoscorites were also subjected to the activity of the ore-forming Ba–Sr–REE orthomagmatic fluids of Ca–Sr–carbonate and REE–hydro–carbonate compositions at temperature ranges of more than 500–480 and 450–430 °C, respectively.

Declaration of Competing Interest

The authors declare that they have no known competing financial interests or personal relationships that could have appeared to influence the work reported in this paper.

Acknowledgements

The work was done on state assignment of IGM SB RAS No. 0330-2016-0002 and GIN SB RAS No. AAAA-A21-121011390002-2. Mineralogical and inclusion investigations were supported by the Russian Science Foundation project No. 19-17-00019.

Appendix A. Supplementary data

Supplementary data to this article can be found online at https://doi.org/10.1016/j.oregeorev.2021.104042.

References

Altmaier, M., Neck, V., Fanghanel, T., 2004. Solubility and colloid formation of Th(IV) in concentrated NaCl and MgCl2 solution. Radiochim. Acta 92, 537–543.
Andreeva, I.A., Kovalenko, V.I., Nikiforov, A.V., Kononkova, N.N., 2007. Compositions of magmas, formation conditions, and genesis of carbonate-bearing ijolites and carbonatites of the Belaya Zima alkaline carbonatite complex, Eastern Sayan. J. Petrol. 15, 551–574. https://doi.org/10.1134/S0869591107060033.
Andreeva, I.A., 2014. Carbonatitic melts in olivine and magnetite from rare-metal carbonatite of the Belaya Zima alkaline carbonatite complex (East Sayan, Russia). Dokl. Earth Sci. 455 (2), 436–440. https://doi.org/10.1134/S1028334X14050018.
Ashchepkov, I., Zhmodik, S., Belyanin, D., Kiseleva, O.N., Medvedev, N., Travin, A., Yudin, D., Karmanov, N.S., Downes, H., 2020. Aillikites and alkali ultramafic lamprophyres of the beloziminsky alkaline ultrabasic-carbonatite massif: possible origin and relations with ore deposits. Minerals 10, 404. https://doi.org/10.3390/min10050404.
Barbosa, E.S.R., Brod, J., Cordiero, P., et al., 2020. Phoscorites of the Salitre I complex: origin and petrogenetic implications. Chem. Geol. 535 https://doi.org/10.1016/j.chemgeo.2020.119463.
Bell, K., Kjarsgaard, B.A., Simonetti, A., 1998. Carbonatites into the twenty–first century. J. Petrol. 39, 1839–1845.
Belov, S.V., Lapin, A.V., Tolstov, A.V., Frolov, A.A., 2008. Metallogeny of Platform Magmatism (Traps, Carbonatites, Kimberlites). SO RAN, Novosibirsk [in Russian].
Brigatti, M.F., Medici, L., Saccani, E., Vaccaro, C., 1996. Crystal chemistry and petrologic significance of Fe3+-rich phlogopite from the Tapira carbonatite complex. Brazil. Am. Mineral. 81, 913–927.
Brod, J., Gaspar, J., De Araújo, D., Gibson, S., Thompson, R., Junqueira-Brod, T., 2001. Phlogopite and tetra-ferriphlogopite from Brazilian carbonatite complexes: petrogenetic constraints and implications for mineral-chemistry systematics. J. Asian Earth Sci. 19, 265–296.
Broom-Fendley, S., Styles, M.T., Appleton, J.D., Gunn, G., Wall, F., 2016. Evidence for dissolution-reprecipitation of apatite and preferential LREE mobility in carbonatite-derived late-stage hydrothermal processes. Am. Mineral. 101, 596–611. https://doi.org/10.2138/am-2016-5502CCBY.
Broom-Fendley, S., Brady, A.E., Wall, F., Gunn, G., Dawes, W., 2017. REE minerals at the Songwe Hill carbonatite, Malawi: HREE-enrichment in late-stage apatite. Ore Geol. Rev. 81, 23–41. https://doi.org/10.1016/j.oregeorev.2016.10.019.
Brown, P.E., 1989. FLINCOR: a microcomputer program for the reduction and investigation of fluid-inclusion data. Am. Mineral. 74 (11), 1390–1393.
Bulakh, A.G., Ivanikov, V.V., Orlova, M.P., 2004. Overview of carbonatite–phoscorite complexes of the Kola Alkaline Province in the context of a Scandinavian North Atlantic Alkaline Province. In: Wall, F., Zaitsev, A.N. (Eds.), Phoscorites and Carbonatites from Mantle toMine: the Key Example of the Kola Alkaline Province. Mineral. Soc., London, pp. 1–43.
Chakhmouradian, A.R., 2006. High-field-strength elements in carbonatitic rocks: geochemistry, crystal chemistry and significance for constraining the sources of carbonatites. Chem. Geol. 235, 138–160.
Chakhmouradian, A.R., Wall, F., 2012. Rare earth elements: minerals, mines, magnets (and more). Elements 8, 333–340.
Chakhmouradian, A.R., Reguir, E.P., Kressall, R.D., Crozier, J., Pisiak, L.K., Sidhu, R., Yang, P., 2015. Carbonatite-hosted niobium deposit at Aley, northern British Columbia (Canada): mineralogy, geochemistry and petrogenesis. Ore Geol. Rev. 64, 642–666. https://doi.org/10.1016/j.oregeorev.2014.04.020.
Chakhmouradian, A.R., Reguir, E.P., Zaitsev, A.N., Couëslan, C., Xu, C., Kynický, J., Mumin, A.H., Yang, P., 2017. Apatite in carbonatitic rocks: compositional variation, zoning, element partitioning and petrogenetic significance. Lithos 274, 188–213.
Cooper, A.F., Collins, A.K., Palin, J.M., Spratt, J., 2015. Mineralogical evolution and REE mobility during crystallisation of ancylite-bearing ferrocarbonatite, Haast River, New Zealand. Lithos 217, 324–337. https://doi.org/10.1016/j.lithos.2015.01.005.
Dalton, J.A., Wood, B.J., 1993. The compositions of primary carbonate melts and their evolution through wall rock reaction in the mantle. Earth and Planet. Sci. Letters. 119, 511–525.
Doroshkevich, A.G., Ripp, G.S., Moore, K.R., 2010. Genesis of the Khaluta alkaline-basic Ba-Sr carbonatite complex (west Transbaikala, Russia). Mineral Petrol 98, 245–268.
Doroshkevich, A.G., Veksler, I.V., Izbrodin, I.A., Ripp, G.S., Khromova, E.A., Posokhov, V.F., Travin, A.V., Vladykin, N.V., 2016. Stable isotope composition of minerals in the Belaya Zima plutonic complex, Russia: implications for the sources of the parental magma and metasomatizing fluids. J. Asian Earth Sci. 116, 81–96. https://doi.org/10.1016/j.jseaes.2015.11.011.
Doroshkevich, A.G., Veksler, I.V., Klemd, R., Khromova, A.E., Izbrodin, I.A., 2017. Trace-element composition of minerals and rocks in the Belaya Zima carbonatite complex (Russia): implications for the mechanisms of magma evolution and carbonatite formation. Lithos 284–285, 91–108.
Doroshkevich, A.G., Chebotarev, D.A., Sharygin, V.V., Prokopyev, I.R., Nikolenko, A.M., 2019. Petrology of alkaline silicate rocks and carbonatites of the Chuktukon massif, Chadobets upland, Russia: sources, evolution and relation to the Triassic Siberian LIP. Lithos 332–333, 245–260.
Ernst, R.E., Bell, K., 2010. Large Igneous Provinces (LIPs) and Carbonatites:. Mineralogy and Petrology. Special issue dedicated to K. Bell and titled "Continental Flood Basalts

and associated igneous complexes 98, 55–76. https://doi.org/10.1007/s00710-009-0074-1.
Ernst, R.E., Hamilton, M.A., Söderlund, U., Hanes, J.A., Gladkochub, D.P., Okrugin, A.V., 2016. Long-lived connection between southern Siberia and 714 northern Laurentia in the Proterozoic. Nat. Geosci. 96, 464–469. https://doi.org/10.1038/NGEO2700.
Frost, B.R., Avchenko, O.V., Chamberlain, K.R., Frost, C.D., 1998. Evidence for extensive proterozoic remobilization of the aldan shield and implications for proterozoic plate tectonic reconstructions of Siberia and Laurentia. Precambr Res 89, 1–23. https://doi.org/10.1016/s0301-9268(97)00074-0.
Giebel, R.J., Marks, M.A.W., Gauert, C.D.K., Markl, G., 2019. A model for the formation of carbonatite–phoscorite assemblages based on the compositional variations of mica and apatite from the Palabora Carbonatite Complex, South Africa. Lithos 324–325, 89–104.
Glagolev, A.A., Korchagin, A.M. and Kharchenkov, A.G., 1974. Arbarastakh and Inagli Alkaline-Ultrabasic Massifs. Nauka, Moscow, 175 pp. [in Russian].
Goroshko, M.V., Guryanov, V.A., 2004. Uranium-rare metal mineralisation in alkaline-ultrabasic masiffs of the south-eastern Siberian Platform. Tikhookeanskaya Geologiya 2, 76–91 [in Russian].
Guzmics, T., Zajacz. Z., 2013. Trace element partitioning between immsicible silicate and carbonate melts, based on natural melt inclusions from Kerimasi volcano, Tanzania. Goldschmidt Conference Abstracts: 1238.
Hamilton, D.L., Kjarsgaard, B.A., 1993. The immiscibility of silicate and carbonate liquids. Afr. Geol. 96 (3), 139–142.
Harlov, D.E., Forster, H.J., Nijland, T.G., 2002. Fluid-induced nucleation of REE-phosphate minerals in apatite: nature and experiment. Part I. Chlorapatite. American Mineralogist 87, 245–261.
Harlov, D.E., Förster, H.-J., 2004. Fluid-induced nucleation of (Y+REE)-phosphate minerals within apatite: Nature and experiment. Part II. Fluorapatite. American Mineralogist 88, 1209–1229. https://doi.org/10.2138/am-2003-8-905.
Hetherington, C.J., Harlov, D.E., 2008. Metasomatic thorite and uraninite inclusions in xenotime and monazite from granitic pegmatites, Hidra anorthosite massif, southwestern Norway: mechanics and fluid chemistry. Am. Mineral. 93, 806–820.
Hogarth, D.D., 1989. Pyrochlore, apatite and amphibole: distinctive minerals in carbonatite. In: Bell, K. (Ed.), Carbonatites. Genesis and Evolution, Unwin Hyman, London, pp. 105–148.
Kogarko, L.N., 2005. The role of global fluids in the genesis of mantle heterogeneities and alkaline magmatism. Geol. Geofiz. 46 (12), 1213–1224.
Kogarko, L.N, Kononova, V.A., Orlova, M.P., Woolley, A.R., 1995. Alkaline Rocks and Carbonatites of the World. Part 2: Former USSR. Chapman & Hall, London, 226.
Kogarko, L., Suddaby, P., Watkins, P., 1997. Geochemical evolution of carbonatite melts in Polar Siberia. Geochem. Int. 35, 113–118.
Kogarko, L.N., Kurat, G., Ntaflos, T., 2007. Henrymeyerite in the metasomatized upper mantle of eastern Antarctica. Canadian Mineralogist 45 (3), 497–501. https://doi.org/10.2113/gscanmin.45.3.497.
Kogarko, L.N., Ryabchikov, I.D., Kuzmin, D.V., 2012. High-Ba mica in olivinites of the Guli massif (Maimecha–Kotui province, Siberia). Russ. Geol. Geophys. 53, 1209–1215.
Kotov, A.B., Glebovitskii, V.A., Kazanskii, V.I., Sal'nikova, E.B., Pertsev, N.N., Kovach, V. P., Yakovleva, S.Z., 2005. Age Boundaries of the Formation of Major Structures in the Central Aldan Shield. Dokl Akad Nauk 405(8):1155–1158 (Dokl. Earth Sci. (Engl. Transl.), 405 (8), 1155–1158.
Kotov, A.B., Salnikova, E.B., Glebovitskii, V.A., Kovach, V.P., Larin, A.M., Velikoslavinskii, S.D., Zagornaya, N.Yu., 2006. Sm–Nd Isotopic Provinces of the Aldan Shield. Dokl Akad Nauk 410(1):91–94 (Dokl. Earth Sci. (Engl. Transl.) 410 (7), 1066–1069).
Kotov, A.B., Skovitina, T.M., Kovach, V.P., Velikoslavinsky, S.D., Lopatin, D.V., Sklyarov, E.V., Tolmacheva, E.V., Bobrovskaya, O.V., 2017. New data on continental crust age in the western part of the Aldan Shield: results of Sm–Nd Isotopic Study of the Cenozoic Sand Deposits in the Chara and Tokkin Basins. Doklady Earth Sci 475(1): 758–761 (Published in Doklady Akademii Nauk, 2015, Vol. 475, No. 3, pp. 291–294 [in Russian]).
Krasnova, N., Balaganskaya, E., Garcia, D., 2004a. Kovdor - classic phoscorites and carbonatites. In: Wall, F., Zaitev, A.N. (Eds.), Phoscorites and Carbonatites from Mantle to Mine: the Key Example of the Kola Alkaline Province. Mineralogical Society of Great Britain and Ireland, London, GB, pp. 99–132.
Krasnova, N., Petrov, T., Balaganskaya, E., Garcia, D., Moutte, J., Zaitsev, A., Wall, F., 2004b. Introduction to phoscorites: occurrence, composition, nomenclature and petrogenesis. In: Wall, F., Zaitev, A.N. (Eds.), Phoscorites and Carbonatites from Mantle to Mine: the Key Example of the Kola Alkaline Province. The Mineralogical Society of Great Britain and Ireland, London, GB, pp. 45–74.
Kuzmin, M.I., Yarmolyuk, V.V., 2014. Mantle plumes of Central Asia (Northeast Asia) and their role in forming endogenous deposits. Russ. Geol. Geophys. 55 (2), 120–143. https://doi.org/10.1016/j.rgg.2014.01.002.
Larin, A.M., Kotov, A.B., Velikoslavinskii, S.D., 2012. Early Precambrian A-granitoids in the Aldan Shield and adjacent mobile belts: sources and geodynamic environments. Petrology 20, 218–239. https://doi.org/10.1134/S0869591112030034.
Le Maitre, R.W., 2002. Igneous Rocks. A Classification and Glossary of Terms, second ed. Cambridge University Press, Cambridge, UK, p. 236.
Leake, B.E., Woolley, A.R., Arps, C.E.S., Birch, W.D., Gilbert, M.C., Grice, J.D., Hawthorne, F.C., Kato, A., Kisch, H.J., Krivovichev, V.G., Linthout, K., Laird, J., Mandarino, J.A., Maresch, W.V., Nickel, E.H., Rock, N.M.S., Schumacher, J.C., Smith, D.C., Stephenson, N.C.N., Ungaretti, L., Whittaker, E.J.W., Youzhi, G., 1997. Nomenclature of amphiboles: Report of the Subcommittee on Amphiboles of the International Mineralogical Association, Commission on New Minerals and Mineral Names. Am. Miner. 82, 1019–1037.
Le Bas, M.J., 1987. Nephelinites and carbonatites. In: Fitton, J. G. Carbonatites—Genesis and Evolution. London: Unwin Hyman, pp. 405– & Upton, B. G. J. (eds) Alkaline Igneous Rocks. Geological Society, London, 427. Special Publication 30, 85–94.
Lee, M.J., Garcia, D., Moutte, J., Lee, J.I., 2003. Phlogopite and tetraferriphlogopite from phoscorite and carbonatite associations in the Sokli massif, Northern Finland. Geosci. J. 7, 9–20.
Mann, U., Marks, M.A.W., Markl, G., 2006. Influence of oxygen fugacity on mineral compositions in peralkaline melts: the Katzenbuckel volcano, Southwest Germany. Lithos 91 (2006), 262–285.
McCormick, G.R., Le Bas, M.J., 1996. Phlogopite crystallization in carbonatitic magmas from Uganda. Can. Mineral. 34, 469–478.
Mitchell, R.H., 1995. Kimberlite, Orangeites and Related Rocks. Plenum Press, New York.
Mitchell, R.H., 2006. Sylvite and fluorite microcrysts, and fluorite–nyerereite intergrowths from natrocarbonatite, Oldoinyo Lengai, Tanzania. Mineral. Mag. 70, 103–114.
Nikolenko, A.M., Redina, A.A., Doroshkevich, A.G., Prokopyev, I.R., Ragozin, A.L., Vladykin, N.V., 2018. The origin of magnetite-apatite rocks of Mushgai-Khudag Complex, South Mongolia: mineral chemistry and studies of melt and fluid inclusions. Lithos 320–321, 567–582. https://doi.org/10.1016/j.lithos.2018.08.030.
Nosova, A.A., Sazonova, L.V., Kargin, A.V., Smirnova, M.D., Lapin, A.V., Shcherbakov, V. D., 2018. Olivine in ultramafic lamprophyres: chemistry, crystallisation, and melt sources of Siberian Pre- and post-trap aillikites. Contrib. Mineral. Petrol. 173, 55. https://doi.org/10.1007/s00410-018-1480-3.
Nosova, A.A., Kargin, A.V., Sazonova, L.V., et al., 2020. Sr-Nd-Pb isotopic systematic and geochronology of ultramafic alkaline magmatism of the southwestern margin of the Siberian Craton: Metasomatism of the sub-continental lithospheric mantle related to subduction and plume events. Lithos. https://doi.org/10.1016/j.lithos.2020.105509.
Osorgin, N.Y., 1990. Chromatographic analysis of the gas phase in minerals (methods, equipment, metrology). Novosibirsk: Preprint N11: 32 [in Russian].
Parfenov, L.M., Kuzmin, M.I., 2001. Tectonics, geodynamics and metallogeny of the territory of the Republic of Sakha (Yakutia). Nauka/Interperiodika, Moscow [in Russian].
Priyatkina, N., Ernst, R., Khudoley, A., 2020. Precambrian Res. 340 https://doi.org/10.1016/j.precamres.2020.105645.
Prokopyev, I.R., Borisenko, A.S., Borovikov, A.A., Pavlova, G.G., 2016. Origin of REE-rich ferrocarbonatites in southern Siberia (Russia): implications based on melt and fluid inclusions. Mineral.
Prokopyev, I.R., Doroshkevich, A.G., Ponomarchuk, A.V., Sergeev, S.A., 2017. Mineralogy, age and genesis of apatite-dolomite ores at the Seligdar apatite deposit (Central Aldan, Russia). Ore Geol. Rev. 81, 296–308. https://doi.org/10.1007/s00710-016-0449-z.
Prokopyev, I.R., Starikova, A.E., Doroshkevich, A.G., Nugumanova, Y.N., Potapov, V.V., 2020. Petrogenesis of ultramafic lamprophyres from the terina complex (Chadobets upland, Russia): Mineralogy and melt inclusion composition. Minerals 10 (5), 419. https://doi.org/10.3390/min10050419.
Rankin, A.H., 2005. Carbonatite-associated rare metal deposits: composition and evolution of ore-forming fluids — the fluid inclusion evidence. In Rare-Element Geochemistry and Mineral Deposits. GAC Short Course Notes 17; Linnen, R. L., Samson, I. M., Eds.; Geological Association of Canada: Quebec, pp. 299–314 ISBN 978-1-897095-08-9.
Rass, I.T., Petrenko, D.B., Koval'chuk, E.V., Yakushev, A.I., 2020. Phoscorites and Carbonatites: Relations, Possible Petrogenetic Processes, and Parental Magma, with Reference to the Kovdor Massif, Kola Peninsula. Geochem. Int. 58 (7), 753–778.
Roedder, E., 1984. Fluid inclusions. REVIEWS in MINERALOGY. Volume 12.; Ribbe, P. H., Ed.; Mineralogical Society of America: Blacksburg, Virginia, USA, 1984; ISBN 978-0-939950-16-4.
Ryabchikov, I.D., Solovova, I.P., Kogarko, L.N., Bray, G.P., Ntaflos, T., Simalin, S., 2002. Thermodynamic parameters of generation of meymechites and alkaline picrites in the Maimecha-Kotui Province: evidence from melt inclusions. Geochem. Int. 40 (11), 1031–1041.
Rosen, O.M., Serenko, V.P., Spetsius, Z.V., Manakov, A.V., Zinchuk, N.N., 2002. Yakutian Kimberlite Province: position in the structure of the Siberian craton and composition of the upperand lower crust. Russ. Geol. Geophys. 43, 1–24.
Redina, A.A., Nikolenko, A.M., Doroshkevich, A.G., Prokopyev, I.R, Wohlgemuth-Ueberwasser, C., Vladykin, N.V., 2020. Conditions for the crystallization of fluorite in the Mushgai-Khudag complex (Southern Mongolia): Evidence from trace element geochemistry and fluid inclusions. Available online 12 June 2020, https://doi.org/10.1016/j.chemer.2020.125666.
Rimskaya-Korsakova, O., Sokolova, E., 1964. About the iron-magnesium micas with the reverse scheme of absorption. Zap. Vses. Mineral. O-va. 93, 411–423 [in Russian].
Rimskaya-Korsakova, O., Krasnova, N., 2002. Geology of the Deposits of Kovdor Massif. St. Petersburg State University, St. Petersburg, Russia, 296 [in Russian].
Rock, N.M.S., 1986. The nature and origin of ultramafic lamprophyres: alnöites and allied rocks. J. Petrol. 27, 155–196.
Shironosova, G.P., Prokopyev, I.R., 2018. Coefficients of distribution of REE+Y between minerals and cooling rich sulfate fluid (thermodynamic modeling). Bull. Tomsk Polytech. Univ.-Geo Assets Eng. 329 (10), 6–18.
Shironosova, G.P., Prokopyev, I.R., 2019. Thermodynamic modeling of REE+Y speciation in cooling sulfatebrich fluids. Bull. Tomsk Polytech. Univ.-Geo Assets Eng. 330 (11), 7–18.
Shu, X., Liu, Y., 2019. Fluid inclusion constraints on the hydrothermal evolution of the Dalucao Carbonatite-related REE deposit, Sichuan Province. China. Ore Geol. Rev. 107, 41–57. https://doi.org/10.1016/j.oregeorev.2019.02.014.

Smith, M.P., Campbell, L.S., Kynicky, J., 2014. A review of the genesis of the world-class Bayan Obo Fe-REE-Nb deposits, Inner Mongolia, China: Multistage processes and outstanding questions. Ore Geol. Rev. 64, 459–476 in this issue.

Tappe, S., Foley, S.F., Jenner, G.A., Kjarsgaard, B.A., 2005. Integrating ultramafic lamprophyres into the IUGS classification of igneous rocks: rationale and implications. J. Petrol. 46, 1893–1900. https://doi.org/10.1093/petro logy/egi03 9.

Tappe, S., Foley, S.F., Jenner, G.A., et al., 2006. Genesis of ultramafic lamprophyres and carbonatites at Aillik Bay, labrador: a consequence of incipient lithospheric thinning beneath the North Atlantic Craton. J. Petrol. 47, 1261–1315. https://doi.org/10.1093/petro logy/egl00 8.

Tropper, P., Manning, C.E., Harlov, D.E., 2011. Solubility of CePO4 monazite and YPO4 xenotime in H2O and H2O–NaCl at 800°C and 1 GPa: implications for REE and Y transport during high-grade metamorphism. Chem. Geol. 282, 58–66.

Tropper, P., Manning, C.E., Harlov, D.E., 2013. Experimental determination of CePO4 and YPO4 solubilities in H2O–NaF at 800°C and 1 GPa: implications for rare earth element transport in high-grade metamorphic fluids. Geofluids 13, 372–380.

Veksler, I.V., Dorfman, A.M., Dulski, P., Kamenetsky, V.S., Danyushevsky, L.V., Jeffries, T., Dingwell, D.B., 2012. Partitioning of elements between silicate melt and immiscible fluoride, chloride, carbonate, phosphate and sulfate melts, with implications to the origin of natrocarbonatite. Geochim. Cosmochim. Acta 79, 20–40.

Velikoslavinskii, S.D., Kotov, A.B., Tolmacheva, E.V., et al., 2011. Early Precambrian granite-gneiss complexes in the Central Aldan Shield. Petrology 19, 382–398. https://doi.org/10.1134/S0869591111040060.

Wall, F., 2013. Critical metals handbook, 10.1002/9781118755341.ch13.

Wall, F., Zaitsev, A.N., 2004. Phoscorites and carbonatites from mantle to mine: the key example of the Kola Alkaline Province. Mineralogical Society Series, 10. Mineralogical Society, London, 498.

Weng, Z., Jowitt, S., Mudd, G., Haqoe, N., 2015. A detailed assessment of global rare earth element resources: opportunities and challenges. Econ. Geol. 110 (8), 1925–1952. https://doi.org/10.2113/econgeo.110.8.1925.

Whitney, D.L., Evans, B.W., 2010. Abbreviations for Names of Rock-Forming Minerals. Am. Mineral. 95 (1), 185–187. https://doi.org/10.2138/am.2010.3371.

Williams-Jones, A.E., Migdisov, A.A., Samson, I.M., 2012. Hydrothermal mobilization of the rare earth elements-a tale of "Ceria" and "Yttria". Elements 8, 355–360.

Woolley, A.R., Kempe D.R.C., 1989. Carbonatites: Nomenclature, average chemical compositions and element distribution. In Carbonatites: Genesis and Evolution. / Unwin Hyman, London, red. Bell K., 1-14.

Woolley, A.R., Kjarsgaard, B.A., 2008. Paragenetic types of carbonatite as indicated by the diversity and relative abundances of associated silicate rocks: evidence from a global database. Can. Mineral. 46, 741–752. https://doi.org/10.3749/canmin.46.4.

Xie, Y., Hou, Z., Yin, S., Dominy, S.C., Xu, J., Tian, S., Xu, W., 2009. Continuous carbonatitic melt–fluid evolution of a REE mineralization system: Evidence from inclusions in the Maoniuping REE Deposit, Western Sichuan. China. Ore Geol. Rev. 36, 90–105. https://doi.org/10.1016/j.oregeorev.2008.10.006.

Yarmolyuk, V.V., Kovalenko, V.I., Sal'nikova, E.B., Nikiforov, A.V., Kotov, A.B., Vladykin, N.V., 2005. Late Riphean rifting and breakup of Laurasia: data on geochronological studies of ultramafic alkaline complexes in the southern framing of the Siberian craton. Dokl. Earth Sci. 404 (7), 1031–1037.

Zheng, X., Liu, Y., 2019. Mechanisms of element precipitation in carbonatite-related rare-earth element deposits: evidence from fluid inclusions in the Maoniuping deposit, Sichuan Province, southwestern China. Ore Geol. Rev. 107, 218–238. https://doi.org/10.1016/j.oregeorev.2019.02.021.